Supplementary Information

Lewis-Acidity-Triggered Active Reconstruction for Cross-Scale Cascade Regulation Enables Industrial CO_2-to-Formate Conversion beyond 1500 h

Na Ye,[1] Kai Wang,[1] Zhengyi Qian,[1] Yingjun Tan,[1] Zheng Lin,[1] Qizheng Huang,[1] Chenglong Sun,[1] Hongyu Guo,[1] Fei Liu,[1] Changshuai Shang,[1] Youxing Liu,[1] Yu Gu,[1] Shipeng Zhang,[1] Lu Li,[1] Ying Han,[1] Chenhui Zhou,[1] Changze Wei,[1] Mingchuan Luo,*[1] Shaojun Guo*[1]

[1]School of Materials Science and Engineering, Peking University, Beijing 100871, P.R. China.

*Correspondence to: guosj@pku.edu.cn and m.luo@pku.edu.cn

Materials. Indium nitrate hydrate ($In(NO_3)_3$, 99.9%) was purchased from Beijing Mreda Technology Co., Ltd. Stannic chloride pentahydrate ($SnCl_4 \cdot 5H_2O$, 99%) was purchased from Shanghai Macklin Biochemical Co., Ltd. Glucose was obtained from Beijing Tong Guang fine chemicals Co. Urea was purchased by Aladdin Reagent Co., Ltd. All chemicals were used without further purification.

Material characterizations. XRD patterns were obtained on a powder X-ray diffractometer (Rigaku D/max-2500) using Cu Kα radiation source (λ = 0.15406 nm). The loading analysis was carried out on an inductively-coupled plasma optical emission spectroscopy (Agilent ICPOES730). HRTEM and HAADF-STEM images were obtained on HITACHI H-7700 and Tecnai G2 F30 S-TWIN, respectively. Oxygen vacancy analysis was obtained on a EPR spectrometer (Bruker A300-10/12). XPS experiments were performed on a ESCALAB 250XI electron spectrometer (Thermo Fisher, Al-Kα X-ray source of 1486.6 eV). FT-IR spectroscopy results were obtained on a Nicolet6700 FT-IR spectrometer.

Electrochemical measurements of CO_2RR. All the electrochemical measurements of CO_2RR were performed by an electrochemical workstation (CHI 660E). In a three-electrode flow cell, CO_2RR performances were conducted in 0.5 M $KHCO_3$ electrolytes with Ag/AgCl as the reference electrode and IrO_x/Ti as the counter electrode. A gas-diffusion electrode (GDE, Sigracet 29BC) with the catalysts ink (1 mg cm^{-2}) brushed on was served as the working electrode, in which the catalysts ink contained catalysts and Nafion (Dupont, 5%). An anion-exchange membrane (Sustainion X37-50 RT) was located to separate the cathode and anode. The applied potentials were calibrated to RHE using the equation ($E_{RHE} = E_{Ag/AgCl} + 0.197\ V + 0.059\ pH - 0.85iR$)[1]. The electrolyte resistance was obtained by electrochemical impedance spectroscopy measurements in the frequency range of 0.1 Hz to 100 kHz. Gaseous products were quantified by a gas chromatography, and liquid products were evaluated using NMR measurements.

In a typical two-electrode MEA electrolyzer (5 cm^2, Dioxide Materials), a IrO_x/Ti foam served as the anode electrode and a GDE (Sigracet 29BC) with the catalysts ink (2 mg cm^{-2}) brushed on served as the cathode electrode, in which the catalysts ink contained catalysts, VXC-72 Cabot black carbon (0.1 mg cm^{-2}) and Nafion (5%). An anion-exchange membrane (Sustainion X37-50 RT) was located to separate the cathode and anode. The anode electrolyte was single-pass 20 mM Cs_2CO_3, and the cathode was supplied with CO_2 behind the GDE. The total amount of products at both the anode and cathode was used to calculate the FE of liquid products. At the cathode outlet, a cold trap was used to collect the liquid products (Supplementary Fig. 23 d). And liquid products were evaluated using HPLC measurements. The system was operated continuously under the same conditions for the full 1500 h without reassembling or disassembling the MEA equipment. During the stability test, to effectively avoid interference from salt precipitation, we implemented a series of strategies in this work, including system restart pretreatment and cathode water flushing prior to the stability test, the use of highly soluble Cs salts, and the continuous use of fresh, low-concentration Cs_2CO_3 electrolyte (Supplementary Fig. 25).

Specifically: 1) At the start of operation, a constant current density of -20 mA cm^{-2} was first applied to the electrolyzer, and then the electrolysis current density was increased stepwise (-50, -100, -200, -300 mA cm^{-2}). Each step was incrementally adjusted after the current had stabilized and gas/liquid product collection was completed, with each step typically requiring an interval of approximately 60 minutes. 2) After ramping up to 300 mA cm^{-2}, a water flush was performed. We found that cleaning without shutdown had a negligible impact on system stability while effectively removing salt precipitates. The specific electrode cleaning method involved injecting a small amount of ultrapure water into the gas line, sufficiently slowly to ensure voltage stability. 3) After the water flush, the cell was operated at 300 mA cm^{-2} for 6 h. When the voltage rose to approximately 3.2 V, the test was stopped. After an interval of 30 s, the test was restarted. This restarted test was recorded as the starting point of the stability test. 4) During the stability test, when the outlet gas flow rate in the

soap-film flowmeter became extremely low or severely uneven, the water flushing operation was initiated, following the same procedure as described above.

Details related to MEA operation were summarized as below.

The active area: 5 cm^2.

The geometric areas of the cathode electrodes: 6.25 cm^2.

The geometric areas of the anode electrodes: 9 cm^2.

The detailed electrode fabrication procedures:

For the cathode, a gas-diffusion electrode (GDE, Sigracet 29BC) with the catalysts ink (1.5 mg cm^{-2}) brushed on was served as the cathode, in which the catalysts ink contained catalysts, VXC-72 Cabot black carbon (0.1 mg cm^{-2}) and Nafion (Dupont, 5%). The mass loading of the cathode catalyst was approximately 1.5 mg cm^{-2}.

For the anode, an IrO_x/Ti was employed as the anode electrode. Typically, the titanium felt (30*30*0.4 mm) was first ultrasonically washed with ultrapure water and acetone, and then etched in 6 M HCl at 70 °C for 40 minutes. After that, 144 mg of iridium dioxide (IrO_2) was dispersed in 36 mL of a mixture of isopropanol and water (volume ratio of 5:1). Then, 1000 μL of Nafion and 320 mg of PTFE emulsion (5 wt%) were added to the mixture to obtain the IrO_2 ink. Subsequently, the as-prepared IrO_2 ink was spray-coated onto the etched titanium felt with a catalyst loading of 2 mg cm^{-2}, followed by calcination in a tube furnace at 350°C for 60 minutes under an Ar atmosphere. Finally, the IrO_x/Ti anode was obtained.

The membrane was soaked in a 1M KOH solution at 80°C for 24 hours and washed 3-4 times with deionized water, to yield an OH^--type alkaline film.

The compression pressure during assembly: around 3.5 kgf·cm.

The presence or absence of CO_2 humidification: the absence of CO_2 humidification.

The gas flow rates: 35 sccm.

The liquid flow rates: 8 mL min^{-1}.

ECSA can be determined based on the double-layer capacitance in the non-faradic region[2,3], as shown in the following Equation S1:

$$ECSA = \frac{C_{dl}}{C_0} \quad \text{(S1)}$$

Where C_{dl} is estimated by the slopes (current *vs* scan rate); C_0 refers to the specific capacitance of an flat surface electrode (40 μF cm^{-2}).

The full-cell energy efficiency signifies the production of formate, as shown in the following Equation S2[4]:

$$EE_{\text{full-cell}} = \frac{(1.23 + (-E^0_{formate})) * FE_{formate}}{-E_{full-cell}} \quad \text{(S2)}$$

Where E_{formate}^0 signifies the thermodynamic potential of CO_2-to-formate conversion; FE_{formate} signifies the formate Faradaic efficiency; $E_{\text{full-cell}}$ signifies full-cell potentials.

The formation rate of formate (FR_{formate}) is calculated by the following Equation S3[5]:

$$FR_{\text{formate}} = \frac{Q_{total} * FE_{formate}}{F * N_{formate} * A * t} = \frac{J_{formate} * 3600}{F * N_{formate}}$$

$$= \frac{300 * 92\% * 3600}{96485 * 2} mmol \cdot h^{-1} \cdot cm^{-2} \quad \text{(S3)}$$

$$= 5.15\ mmol \cdot h^{-1} \cdot cm^{-2}$$

$$= 5.15 * 1500 * 5\ mmol = 38625\ mmol$$

Where Q_{total} signifies the overall charge (C); F is the Faradaic constant (96485 C mol^{-1}); $N_{formate}$ is 2 that represents the transferred electron numbers for formate products; A signifies the electrode area (cm^2); t is the electrolysis time (h); $J_{formate}$ is the formate partial current densities (mA cm^{-2}).

DFT calculations. DFT calculations were performed by the implement of the Vienna *Ab initio* Simulation Package (VASP)[6,7] along with the Perdew-Burke-Ernzerhof functional[8,9]. The projector-augmented wave (PAW) pseudo-potentials were applied to clarify the electronic exchange interactions[10] with the energy convergence threshold of 10^{-5} eV and geometry relaxation of 0.02 eV/Å. The Brillouin zone was sampled by employing a Monkhorst-Pack k-point mesh of 3 ×3 × 1. A 15 Å z-direction vacuum layer was applied to isolate adjacent slabs. Models in this work were employed based on the EXAFS results. In the AIMD calculations, the hydrogen atoms in the system were replaced with deuterium atoms and the time step of 1.0 fs was employed. Simulations were conducted within the canonical ensemble (NVT) using a Nose-Hoover chain thermostat to maintain a target temperature of 300 K. An initial equilibration period of 3 ps was followed by a 7 ps production phase for the subsequent sampling. A plane-wave cutoff energy of 400 eV was employed. And only the gamma point in reciprocal space was employed. The three surface atomic layers and H_2O molecules were fully relaxed. Ionic relaxations were performed with the energy of 10^{-4} eV.

The overall CO_2RR-to-formate synthesis considered are shown using the following equations:

$$CO_2 + * \rightarrow *CO_2$$

$$*CO_2 + 2H_2O + 2e^- \rightarrow *OCHO + 2OH^- \quad \text{(S4-7)}$$

$$*OCHO + H_2O + e^- + OH^- \rightarrow *HCOOH + 2OH^-$$

$$*HCOOH + 2OH^- \rightarrow HCOOH + * + 2OH^-$$

Where * indicates the adsorption sites.

The Gibbs free energy change (ΔG) can be calculated (298.15 K, 1 atm) with the equation below:

$$\Delta G = \Delta E_{DFT} + \Delta E_{ZPE} + \Delta G_U - T\Delta S \quad \text{(S8)}$$

Where ΔE_{DFT}, ΔE_{ZPE}, and ΔS denote the total energy difference based on the DFT calculations, the zero-point vibrational energy and the entropy change, respectively. ΔG_U is defined as -eU, where e indicates the elementary charge and U denotes the electrode potential.

The adsorption energy E_{ads} can be calculated employing the following equation:

$$E_{ads} = E_{\text{adsorbate-slab}} - (E_{\text{adsorbate}} + E_{slab}) \quad \text{(S9)}$$

Where $E_{\text{adsorbate-slab}}$ denotes the energy of the model with adsorbates adsorbed on the surface, E_{slab} and $E_{\text{adsorbate}}$ indicate the energies of optimized clean slab surface and isolated adsorbates, respectively.

TEA analysis of the CO_2RR-to-HCOOCs process in MEA (300 mA cm^{-2})

We did a quantitatively techno-economic analysis (TEA) for formate production in MEA cell systems, based on a modified model from previous reports, incorporating the performance obtained from our experimental results[11-13].

For HCOOCs production, the production of 1 mole of HCOOCs necessitates the consumption of 1 mole of CO_2, 1 mole of H_2O and 0.5 mole of Cs_2CO_3. We assumed a cost analysis for the production of 100,000 kg of HCOOCs *per* day with a capacity factor of 0.9 (32,850 tons *per* year = 100000*0.9*365/1000), considering a factory lifespan of 20 years[12,14,15].

For this estimation, we used experimentally derived data from our long-term experiments to approximate the operating conditions of a potential industrial electrolyzer. For HCOOCs production in a MEA electrolyzer, the process was operating at a total current of 300 mA cm^{-2} with FE of 92.0% with a cell voltage of 3 V. There is no need for catholyte, while 20 mM Cs_2CO_3 solution was used as the anolyte.

For HCOOCs production, the partial current needed is:

$$I_{HCOOCs}=100{,}000\frac{kg}{day}*\frac{day}{86{,}400\ s}*1{,}000\frac{g}{kg}*\frac{mol}{177.92}*2\ e^{-}*96{,}485\frac{C}{mol}=1{,}255{,}310.86\ A$$

The total current needed is the partial current divided by the faradaic efficiency:

$$I_{total}=\frac{1{,}255{,}310.86\ A}{0.92}=1{,}364{,}468.33\ A$$

The electrolyzer area needed is the total current divided by the current density:

$$Total\ electrolyzer\ area=\frac{1{,}364{,}468.33\ A}{0.3\ \frac{A}{cm^2}}*\frac{m^2}{10{,}000\ cm^2}=454.82\ m^2$$

The power needed is given from P=VI:

$$Power=3\ V*1{,}364{,}468.33\ A*\frac{kW}{1{,}000\ W}=4{,}093.40\ kW$$

The CO_2 flow rate needed is:

$$CO_2\ flow=100{,}000\frac{kg}{day}*1{,}000\frac{g}{kg}*\frac{mol}{177.92}=562{,}050.36\ \frac{mol}{day}=24{,}730.22\ \frac{kg}{day}$$

According to 65% single pass conversion efficiency of CO_2, the inlet flow rate and outlet flow rate of CO_2 are:

$$CO_2\ inlet\ flow=562{,}050.36\frac{mol}{day}*\frac{day}{24\ h}*\frac{1}{0.65}=36{,}028.87\ \frac{mol}{h}=1{,}585.27\ \frac{kg}{h}$$

$$CO_2\ outlet\ flow=36{,}029.87\ \frac{mol}{h}*(1\text{-}0.65)=12{,}610.10\ \frac{mol}{h}=554.84\ \frac{kg}{h}$$

$$CO_2\ Outlet\ flow\ rate=\frac{CO_2\ outlet\ flow*R*T}{P}=\frac{12{,}610.10\ \frac{mol}{h}*8.314\ \frac{J}{mol\ K}*298\ K}{101\ kPa}=309.33\left(\frac{m^3}{h}\right)$$

The byproduct is hydrogen (FE=8%), and the flow rate of hydrogen is:

$$H_2\ production\ rate=1{,}364{,}468.33*3{,}600\frac{s}{h}*0.08*\frac{1}{2\ e^{-}*96{,}485\frac{C}{mol}}=2{,}036.41\ \frac{mol}{h}$$

$$H_2\ flow\ rate=\frac{H_2\ production\ rate*R*T}{P}=\frac{2{,}036.41\ \frac{mol}{h}*8.314\ \frac{J}{mol\ K}*298\ K}{101\ kPa}=49.95\left(\frac{m^3}{h}\right)$$

The water flow rate for the anodic OER reaction is:

$$Anodic\ H_2O\ flow\ rate = 1{,}364{,}468.33\ A * 3{,}600\ \frac{s}{\text{h}} * \frac{1}{2\ e^- * 96{,}485\ \frac{C}{mol}} * 0.018\ \frac{kg}{mol} = 458.19\ \frac{kg}{\text{h}}$$

The liquid HCOOCs product flow rate is:

$$liquid\ product\ flow\ rate = 100{,}000\ \frac{kg}{day} * \frac{day}{24\ \text{h}} * 1{,}000\ \frac{g}{kg} * \frac{mol}{177.92} * \frac{1}{0.02\ \frac{mol}{L}} = 1{,}170{,}938.25\ \frac{L}{\text{h}}$$

1. Electolyzer cost

We referenced the analysis re-calculated based on the stack cost from DOE Current Central H2A PEM electrolysis. The reference electrolyzer cost for the stack component was 550 USD kW^{-1}, and it operated at 1.75 V and 0.4 A cm^{-2} [15-17]. In PEM systems, the precious Ir anode catalyst (2 mg cm^{-2}) dominates electrode cost; our electrolyzer is inferred to have a similar cost structure. To compare configurations with different power densities fairly, costs were recalculated per area (USD m^{-2}) rather than per power (USD kW^{-1}). Based on the DOE H2A PEM model, the electrolyzer cost *per* m^2 is calculated as follows:

$$Electrolyzer\ cost_{\text{per m}^2} = Reported\ cost\ \left(\frac{USD}{kW}\right) * Reported\ power\ density\ \left(\frac{kW}{m^2}\right)$$

$$= 550\ \left(\frac{USD}{kW}\right) * \frac{0.4\ A}{cm^2} * 1.75 V * \frac{kW}{10^3\ W} * \frac{10^4\ cm^2}{m^2} = 3{,}850.00\ \frac{USD}{m^2}$$

According to the factory operation capacity factor of 0.9, which represents the ratio of practical production to the maximum potential production capacity, the electrolyzer cost can be calculated as below[12].

$$Electrolyzer\ cost = Total\ electrolyzer\ area * Electrolyzer\ cost_{\text{per m}^2}$$

$$= 454.82\ m^2 * 3{,}850.00\ \frac{USD}{m^2} = 1{,}751{,}057.00\ USD$$

Assuming a capital discount rate (i) of 5%, the capital recovery factor (CRF) can be calculated as below:

$$CRF_{electrolyzer} = \frac{i(1+i)^{lifetime}}{(1+i)^{lifetime} - 1} = \frac{0.05 * (1+0.05)^{20}}{(1+0.05)^{20} - 1} = 0.08$$

$$Electrolyzer\ cost_{per\ ton\ HCOOCs} = 1{,}751{,}057.00 * \frac{0.08}{365 * 0.9} * \frac{1}{100\ \left(\frac{ton\ \text{HCOOCs}}{day}\right)} = 4.26\ \frac{USD}{ton}$$

2. Balance of plant cost

According to the DOE H2A analysis for distributed grid electrolysis, the Balance of Plant (BOP) cost, which including both mechanical components BoP and electrical BoP, is 39% of the total cost, while the stack is 61% [11]. Thus, the total BoP capital cost is:

$$BoP\ cost = Electrolyzer\ cost\ (USD) * \frac{0.39}{0.61} = 1{,}751{,}057.00\ USD * \frac{0.39}{0.61} = 1{,}119{,}528.25\ \text{USD}$$

Herein, the BOP capital cost for production of *per* ton HCOOCs can be calculated as below:

$$BoP\ cost_{per\ ton\ HCOOCs} = 1{,}119{,}528.25\ USD * \frac{0.08}{365 * 0.9} * \frac{1}{100\ \left(\frac{ton\ \text{HCOOCs}}{day}\right)} = 2.73\ \frac{USD}{ton}$$

3. Electricity cost

We estimate the cost of electricity using the average industrial electricity price of US in 2024, which is 0.08 USD *per* kilowatt-hour as informed by data from the Department of Energy (DOE)[18]. To calculate the electricity cost *per* ton of formate, we divided the total electricity cost by the daily output of production.

$$Cost_{electricity}=\frac{Power\times 24\ \frac{\mathrm{h}}{day}\times price_{electricity}}{HCOOCs\ production}=\frac{4{,}093.40\ kW\times 24\ \frac{\mathrm{h}}{day}\times\frac{0.08\ USD}{kW\mathrm{h}}}{100\left(\frac{ton\ \mathrm{HCOOCs}}{day}\right)}=78.59\ \frac{USD}{ton}$$

4. Pressure-swing adsorption (PSA) cost

To enhance the recirculation of unreacted CO_2, byproduct H_2 is separated from the CO_2 outlet stream. To estimate the costs of gaseous separation, we refer to data from a reference pressure-swing adsorption (PSA) system[12]. The model uses a reference cost of $1,989,043 for a flowrate capacity of 1000 $m^3\ h^{-1}$ with a scaling factor of 0.7 and an energy consumption of 0.25 kWh m^{-3} [19].

$$PSA\ capital\ cost=reference\ cost*\left(\frac{total\ flow\ rate}{reference\ capacity}\right)^{scale\ factor}=1{,}989{,}043\ USD*\left(\frac{309.33\ \frac{m^3}{\mathrm{h}}+49.95\ \frac{m^3}{\mathrm{h}}}{1000\ \frac{m^3}{\mathrm{h}}}\right)^{0.7}$$

$$=971{,}510.06\ USD$$

$$PSA\ capital\ cost_{per\ ton\ HCOOCs}=971{,}510.06\ USD*\frac{0.08}{365*0.9}*\frac{1{,}000\ \frac{kg}{ton}}{100{,}000\ \frac{kg}{day}}=2.37\ \frac{USD}{ton}$$

$$PSA\ operating\ cost=\frac{total\ flow\ rate*\ reference\ PSA\ cost*electricity\ price}{target\ output\ production}=$$

$$\frac{\left(309.33\ \frac{m^3}{\mathrm{h}}+49.95\ \frac{m^3}{\mathrm{h}}\right)*24\ \frac{\mathrm{h}}{day}*0.25\ \frac{kW\mathrm{h}}{m^3}*0.08\ \frac{USD}{kW\mathrm{h}}}{100\ \frac{ton\ HCOOCs}{day}}=1.72\ \frac{USD}{ton}$$

$$PSA\ total\ cost=PSA\ capital\ cost+PSA\ operating\ cost=4.09\ \frac{USD}{ton}$$

5. Liquid product separation cost

Membrane concentration coupled with vacuum fractional crystallization is a low-energy separation alternative to distillation for CO_2RR-derived cesium formate. The mixed electrolyte containing cesium formate and residual cesium carbonate first undergoes reverse osmosis to remove bulk water, followed by MVP vacuum crystallization. Selective separation of the two salts is achieved via their distinct solubility gaps under vacuum, yielding ≥98% pure solid cesium formate. Distillation is infeasible for this inorganic salt mixture due to the absence of usable vapor-liquid separation properties. Carbonate-rich mother liquor is fully recycled to the electrolyzer, cutting electrolyte loss and fitting streamlined techno-economic evaluation[14,20,21].

RO cost:

The liquid HCOOCs product flow rate is:

$$liquid\ product\ flow\ rate = 100{,}000\ \frac{kg}{day} * \frac{day}{24\ \text{h}} * 1{,}000\ \frac{g}{kg} * \frac{mol}{177.92} * \frac{1}{0.02\ \frac{mol}{L}} = 1{,}170{,}938.25\ \frac{L}{\text{h}}$$

Based on the average flux for RO membrane of 50 L m^{-2} h^{-1} [21]. Area of RO:

$$Area = \frac{1{,}170{,}938.25\ \frac{L}{\text{h}}}{50\ \text{L m}^{-2}\ \text{h}^{-1}} = 23418.765\ m^2$$

The cost of commercial RO modules was estimated at 380 USD m^{-2}, based on pricing data from DuPont Filmtec SW30-2521 (AUD 475 *per* unit with 0.7432 m^2 membrane area; ~428 USD m^{-2})[21].

$$RO\ capital\ cost = 23418.765\ m^2\ * 380 \frac{USD}{m^2} + \text{BOP} = 8{,}899{,}130.70 * 2\ \frac{USD}{m^2}$$

$$= 17{,}798{,}261.40\ \frac{USD}{m^2}$$

$$CRF_{RO\text{-}M} = \frac{i(1+i)^{lifetime}}{(1+i)^{lifetime}-1} = \frac{0.05*(1+0.05)^5}{(1+0.05)^5-1} = 0.23$$

$$CRF_{RO\text{-}BOP} = \frac{i(1+i)^{lifetime}}{(1+i)^{lifetime}-1} = \frac{0.05*(1+0.05)^{10}}{(1+0.05)^{10}-1} = 0.13$$

$$\text{RO } capital\ cost_{per\ ton\ HCOOCs} = 8{,}899{,}130.70\ USD * \frac{0.23}{365*0.9} * \frac{1}{100\left(\frac{ton}{day}\right)} + 8{,}899{,}130.70\ USD * \frac{0.13}{365*0.9} * \frac{1}{100\left(\frac{ton}{day}\right)}$$

$$= 62.31 + 35.21\ \frac{USD}{ton} = 97.52\ \frac{USD}{ton}$$

According to the reference[21], the electricity consumption for RO is 4.5 kWh to produce 1,000 kg of RO water.

The liquid HCOOCs product flow rate is:

$$liquid\ product\ flow\ rate = 100{,}000\ \frac{kg}{day} * \frac{day}{24\ \text{h}} * 1{,}000\ \frac{g}{kg} * \frac{mol}{177.92} * \frac{1}{0.02\ \frac{mol}{L}} = 1{,}170{,}938.25\ \frac{L}{\text{h}}$$

The feed flow rate of dilute cesium formate solution is 1,170,938.25 L/h, with an initial cesium formate concentration of 40 mM (0.04 mol/L), and the target concentration after RO concentration treatment is 1 mol/L. The total mass of solute remains constant throughout the concentration process in accordance with material balance.

Taking the approximate density of water as 1 kg/L for dilute aqueous solutions to convert volume to mass, the mass of water required to be evaporated/removed from the system *per* hour is determined to be:

$$M_{H_2O} = \rho_{H_2O} * V_{liquid\ product\ flow\ rate} \frac{C_{outlet} - C_{input}}{C_{outlet}} = 1\ \frac{kg}{L} * 1{,}170{,}938.25\ \frac{L}{\text{h}} * \frac{1\ \frac{mol}{L} - 0.04\ \frac{mol}{L}}{1\ \frac{mol}{L}} = 1{,}124{,}100.72\ \frac{kg}{h}$$

$$\text{RO electricity} = \frac{liquid\ product\ flow\ rate}{1000} * \text{Electricity}_{\text{RO module}}\ (\text{kwh day-1}) * \text{Price}$$

$$= 1{,}124{,}100.72\ \frac{kg}{h} * 4.5\ \frac{\text{kwh}}{1{,}000\ kg} * 0.08\ \frac{USD}{kWh} = 404.68\ \frac{USD}{\text{h}}$$

RO electricity$_{per\ ton\ HCOOCs}$ = 404.68 $\frac{USD}{\mathrm{h}}$*24 $\frac{h}{\mathrm{day}}$*$\frac{1}{100\left(\frac{ton}{day}\right)}$ = 97.12$\frac{USD}{ton}$

According to the reference[21], RO maintenance rate is 2% year^{-1}.

RO maintenance$_{per\ ton\ HCOOCs}$ = *RO capital cost* * RO maintenance rate

=17,798,261.40 USD*$\frac{0.02}{365*0.9}$*$\frac{1}{100\left(\frac{ton}{day}\right)}$ = 10.84 USD/ton

$$RO\ operating\ Cost_{per\ ton\ HCOOCs} = \text{RO electricity}_{per\ ton\ HCOOCs} + \text{RO maintenance}_{per\ ton\ HCOOCs}$$
$$= 97.12\ \frac{USD}{ton} + 10.84\ \frac{USD}{ton} = 107.96\frac{USD}{ton}$$

$$RO\ Cost_{per\ ton\ HCOOCs} = \text{RO } capital\ cost_{per\ ton\ HCOOCs} + RO\ operating\ Cost_{per\ ton\ HCOOCs}$$
$$= 97.52\ \frac{USD}{ton} + 107.96\ \frac{USD}{ton} = 205.48\ \frac{USD}{ton}$$

Distillation cost:

According to the reference[20], the capital cost of evaporative crystallization equipment is quantified via the simplified fitted linear expression derived from the equipment cost-capacity curve[20]: Y=64.8+59.5X. where Y denotes the equipment price in ten thousand Chinese Yuan (CNY), and X represents the water treatment capacity in ton *per* hour (t/h).

$$water\ treatment\ capacity_{Evaporative\ crystallization} = \frac{\rho * C_{input} * V}{1000 * C_{outlet}} = \frac{1\frac{kg}{L} * 0.04\frac{mol}{L} * 1{,}170{,}938.25\frac{L}{\mathrm{h}}}{1000 * 1\frac{mol}{L}} = 46.84\ \frac{ton}{h}$$

Evaporative crystallization capital cost = 64.8+59.5*46.84=*2851.78CNY/6.8 USD =419.38 USD*

Evaporative crystallization$_{capital\ cost\text{-}BOP}$*=419.38 USD *5%=20.97 USD*

Evaporative crystallization$_{capital\ cost}$ = 419.38+20.97=440.35 USD

$$Evaporative\ crystallization\ cost_{per\ ton\ HCOOCs} = 440.35\ USD * \frac{0.08}{365*0.9} * \frac{1}{100\left(\frac{ton}{day}\right)} = 0.0011\ \frac{USD}{ton}$$

Evaporative crystallization Operating cost= 96.37 CNY/t=14.17 USD/t

$$Evaporative\ crystallization\ Cost_{per\ ton\ HCOOCs} = 0.0011\ \frac{USD}{ton} + 14.17\ \frac{USD}{ton} = 14.17\ \frac{USD}{ton}$$

Liquid product separation cost = $RO\ Cost_{per\ ton\ HCOOCs}$*2 + $Evaporative\ crystallization\ Cost_{per\ ton\ HCOOCs}$

=205.48*2 $\frac{USD}{ton}$ + 14.17 $\frac{USD}{ton}$

=425.13 $\frac{USD}{ton}$

6. Catalyst and membrane cost

As mentioned above, the Ir catalyst used for the anodic water oxidation reaction (WOR) constitutes a significant portion of the electrolyzer cost. It is assumed that the costs of the catalyst and membrane

account for 50% of the total electrolyzer cost, and that the catalyst and membrane have a lifetime of 5 years[13,15].

$$CRF_{C\&M} = \frac{i(1+i)^{lifetime}}{(1+i)^{lifetime}-1} = \frac{0.05(1.05)^5}{(1.05)^5-1} = 0.23$$

$$Cost_{C\&M} = \frac{CRF_{C\&M} * Cost_{Total\ Electrolyzer}\ (USD) * 50\%}{Capacity\ factor * 365\left(\frac{days}{year}\right) * production\left(\frac{ton}{day}\right)} = \frac{0.23 * 1{,}751{,}057.00\ USD * 50\%}{0.9 * 365\left(\frac{days}{year}\right) * 100\left(\frac{ton}{day}\right)} = 6.13\ \frac{USD}{ton}$$

7. Input chemical cost

The cost of input CO_2 can be calculated by multiply CO_2 consumption by a market price for CO_2 (40 USD ton^{-1})[11,15].

$$Input\ CO_2\ cost = 40\frac{USD}{ton\ CO_2} * 24{,}730.22\ \frac{kg\ CO_2}{day} * \frac{ton}{1{,}000\ kg} * \frac{1}{100\frac{ton}{day}} = 9.89\ \frac{USD}{ton}$$

Water consumption can be approximated by the anodic H_2O flow rate, given that the water from the cathodic liquid product flow rate is recyclable. Therefore, the cost of input H_2O can be calculated by multiply water consumption by a market price for water (5 USD ton^{-1})[12].

$$Input\ H_2O\ cost = 5\frac{USD}{ton\ H_2O} * 458.19\ \frac{kg\ H_2O}{\text{h}} * \frac{ton}{1{,}000\ kg} * 24\frac{\text{h}}{day} * \frac{1}{100\frac{ton}{day}} = 0.55\ \frac{USD}{ton}$$

For HCOOCs production, the electrolyte is 0.02 mol L^{-1} Cs_2CO_3. The market price of Cs_2CO_3 and HCOOCs are taken as 294,117.65 and 411,764.71 USD ton^{-1}, respectively, with price data from 1688.com. As mentioned above, the production of 1 mole of HCOOCs necessitates the consumption 1 mole of Cs^+, the electrolyte Cs_2CO_3 cost can be calculated as:

$$Mass_{Cs_2CO_3} = 1\ ton\ HCOOCs * \frac{1{,}000{,}000\ g}{ton} * \frac{mol}{177.92\ g} * \frac{325.82\ g}{2\ mol\ Cs^+} * \frac{ton}{1{,}000{,}000\ g} = 0.92\ ton$$

$$Cs_2CO_3\ cost_{per\ ton\ HCOOCs} = 0.92\ ton * 294{,}117.65\frac{USD}{ton} = 270{,}588.24\ \frac{USD}{ton}$$

8. Other operational cost

Other operational cost, including pre-treat, labor and maintenance, are presumed to constitute 2% of the electricity's cost[12,13,15].

$$Other\ cost_{per\ ton\ HCOOCs} = 78.59\ \frac{USD}{ton} * 0.02 = 1.57\ \frac{USD}{ton}$$

9. Total cost for one ton of Product:

By summing all the above costs, the cost for producing one ton of formate can be obtained:

For HCOOCs:

$$Cost_{HCOOCs} = Cost_{electrolyzer} + Cost_{BoP} + Cost_{electricity} + Cost_{PSA} + Cost_{Liquid\ product\ separation} + Cost_{catalyst\ and\ membrane} + Cost_{CO_2} + Cost_{water} + Cost_{Electrolyte\ Cs_2CO_3} + Cost_{other}$$

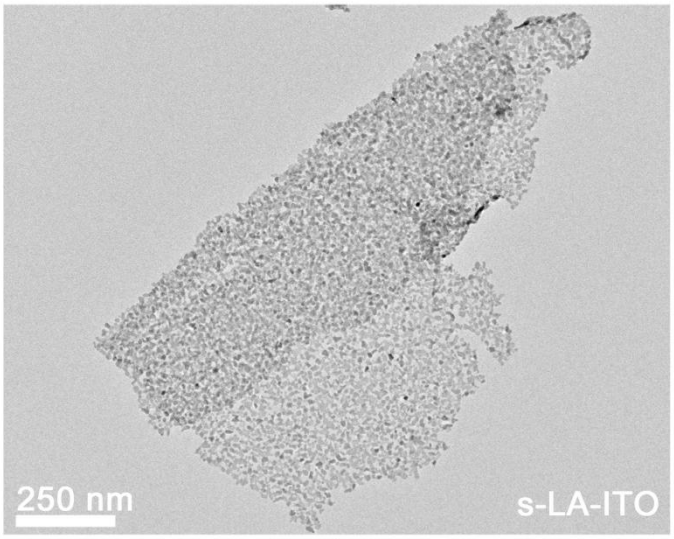
$$= 4.26 + 2.73 + 78.59 + 4.09 + 425.13 + 6.13 + 9.89 + 0.55 + 270{,}588.24 + 1.57 = 271{,}121.18\ \frac{USD}{ton}$$

10. Profit:

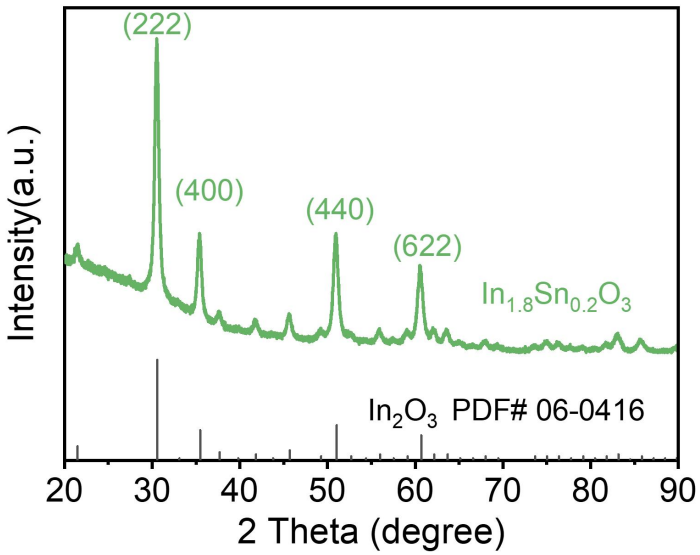
$$Profit = HCOOCs_{\text{per ton HCOOCs}} - Cost_{HCOOCs}$$

$$= 411{,}764.71 \ \frac{USD}{ton} - 271{,}121.18 \ \frac{USD}{ton} = 140{,}643.53 \ \frac{USD}{ton}$$

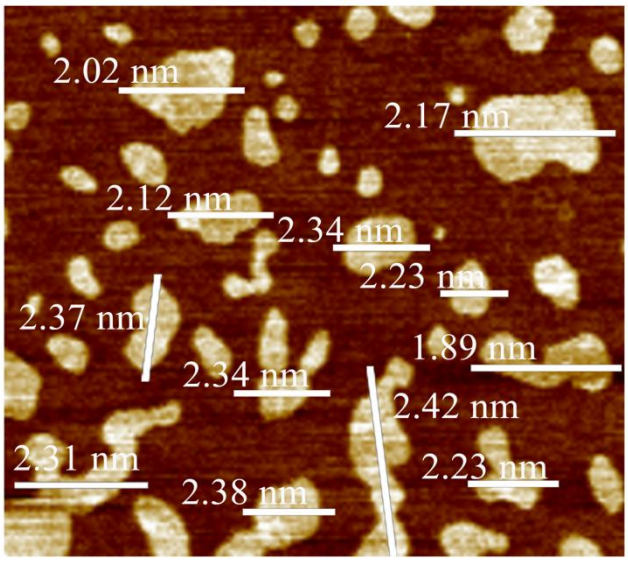
Figures



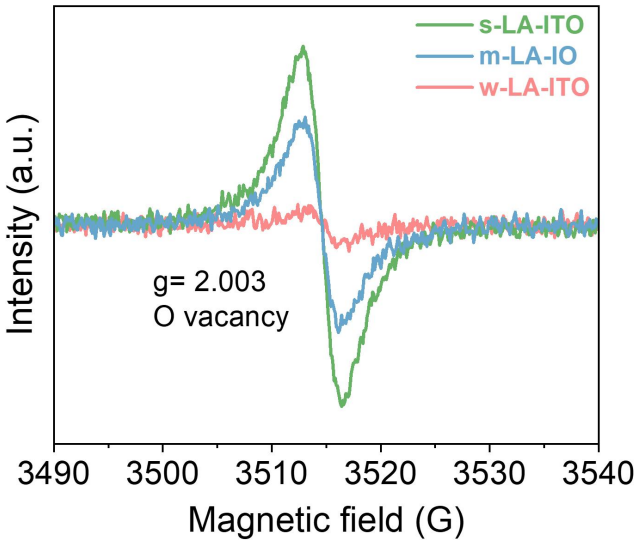
Supplementary Fig. 1 | TEM image of the pre-catalyst of $In_{1.8}Sn_{0.2}O_3$ nanosheets (s-LA-ITO).



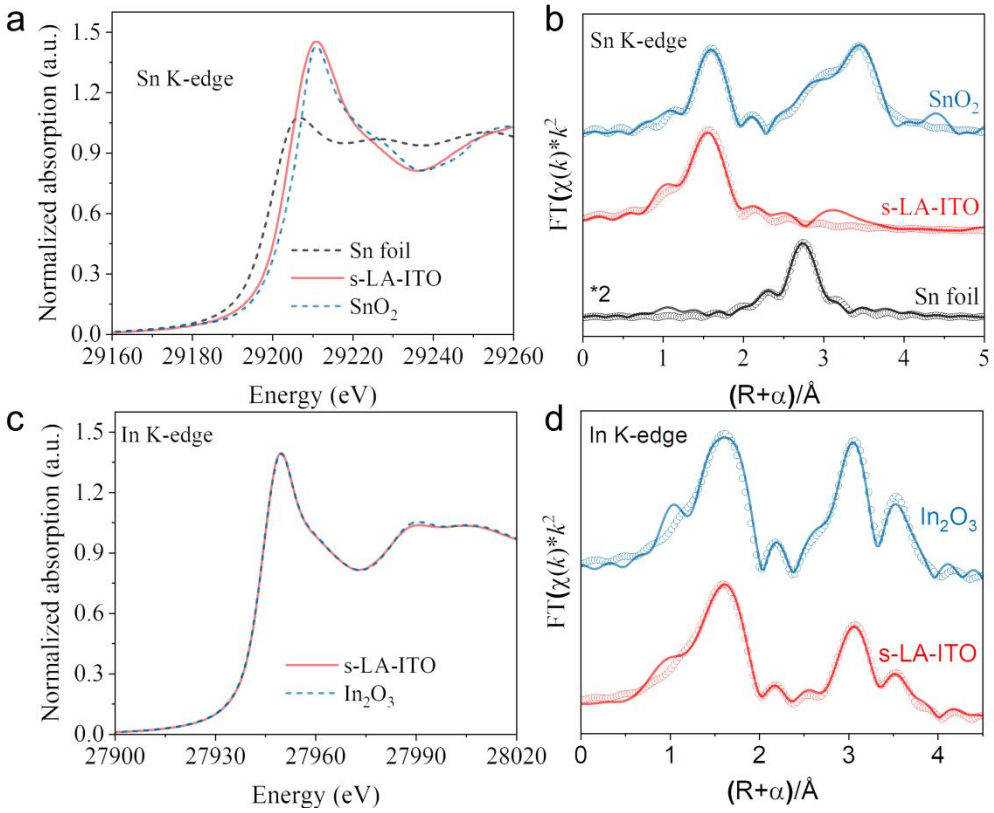
Supplementary Fig. 2 | XRD pattern of the pre-catalyst of $In_{1.8}Sn_{0.2}O_3$ nanosheets.



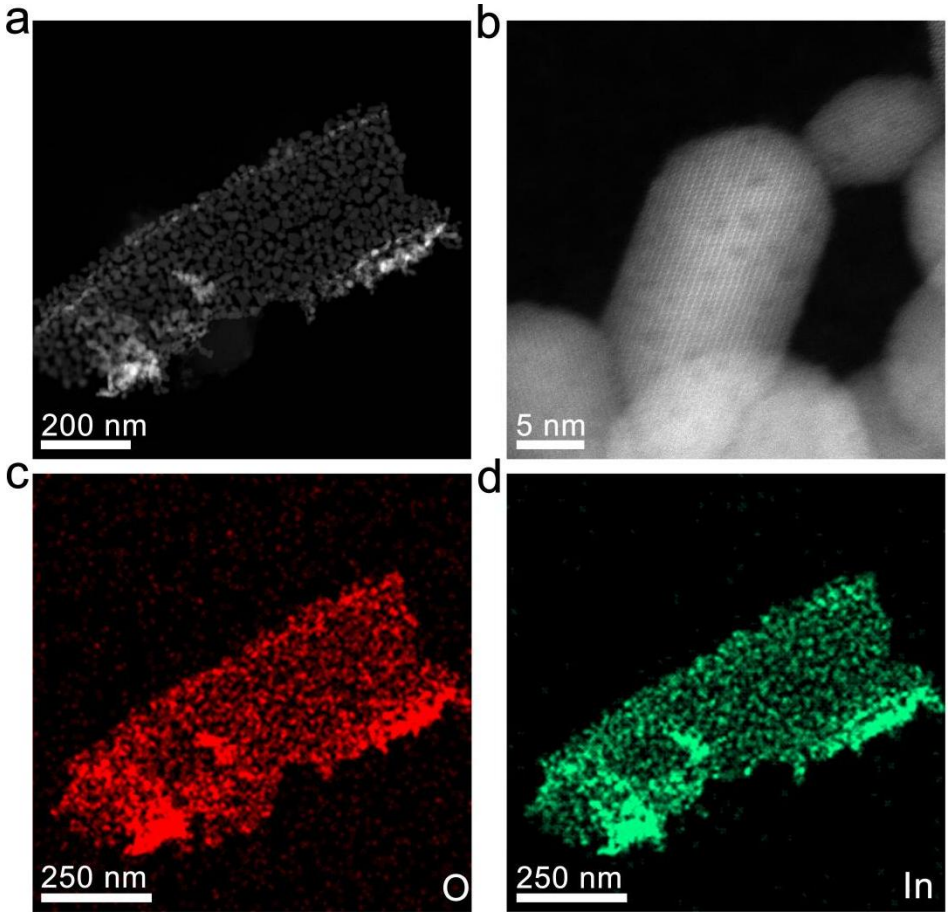
Supplementary Fig. 3 | AFM image of the pre-catalyst of s-LA-ITO.



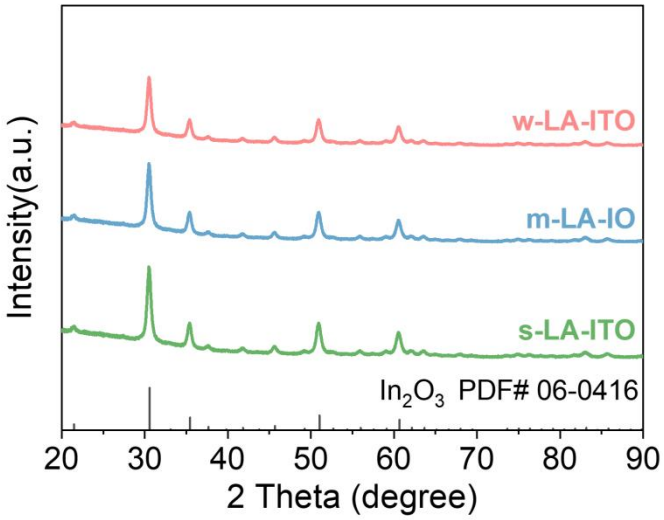
Supplementary Fig. 4 | EPR spectra of s-LA-ITO, m-LA-IO and w-LA-ITO.



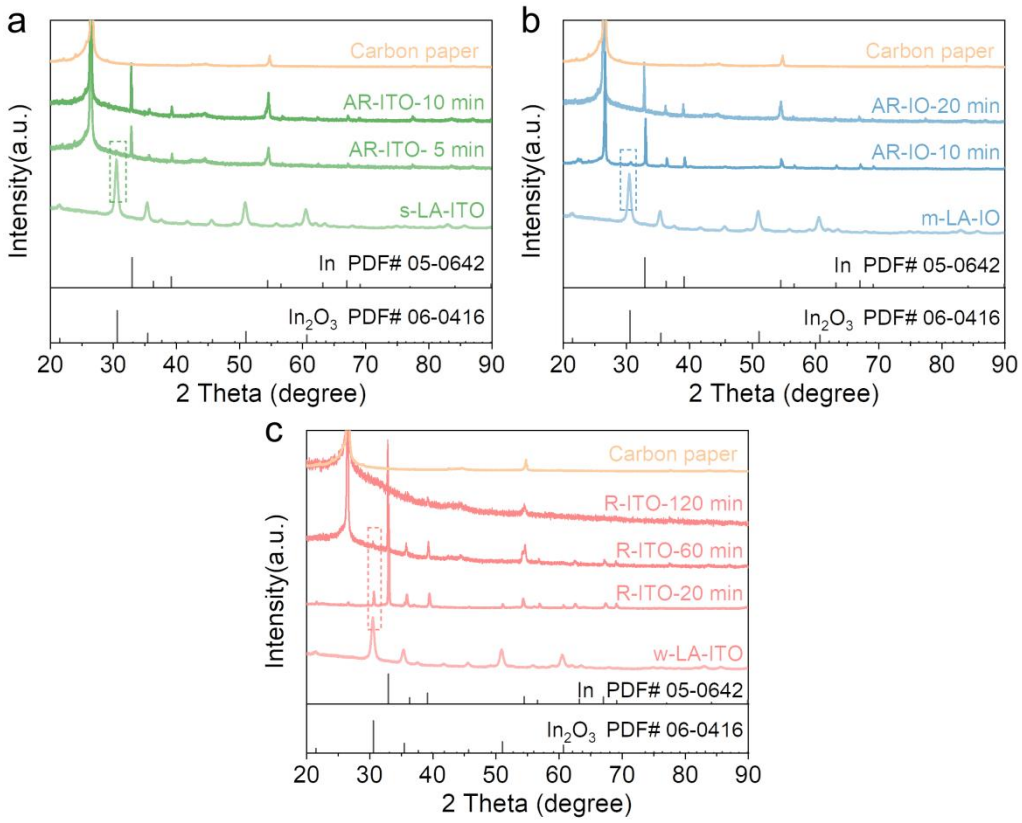
Supplementary Fig. 5 | **a** Normalized Sn *k*-edge XANES spectra of s-LA-ITO, SnO_2, and Sn foil. **b** Fourier transform of In *k*-edge EXAFS spectra (solid line) and corresponding fitting curves (circles) at R space of s-LA-ITO, SnO_2, and Sn foil. The data were *k*3-weighted and not phase-corrected. **c** Normalized In *k*-edge XANES spectra of s-LA-ITO and In_2O_3. **d** Fourier transform of In *k*-edge EXAFS spectra (solid line) and corresponding fitting curves (circles) at R space of s-LA-ITO and In_2O_3. The data were *k*3-weighted and not phase-corrected.



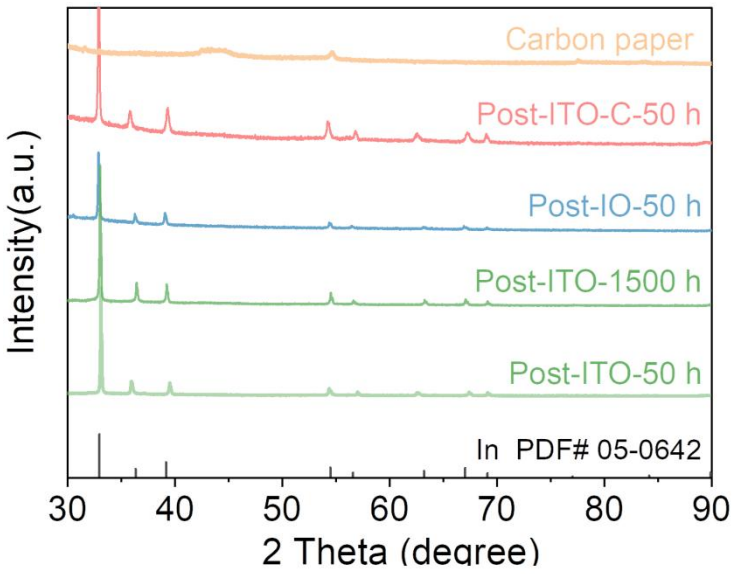
Supplementary Fig. 6 | **a** HR-TEM image, **b** HAADF-STEM image and **c-d** EDS elemental mapping images of In_2O_3.



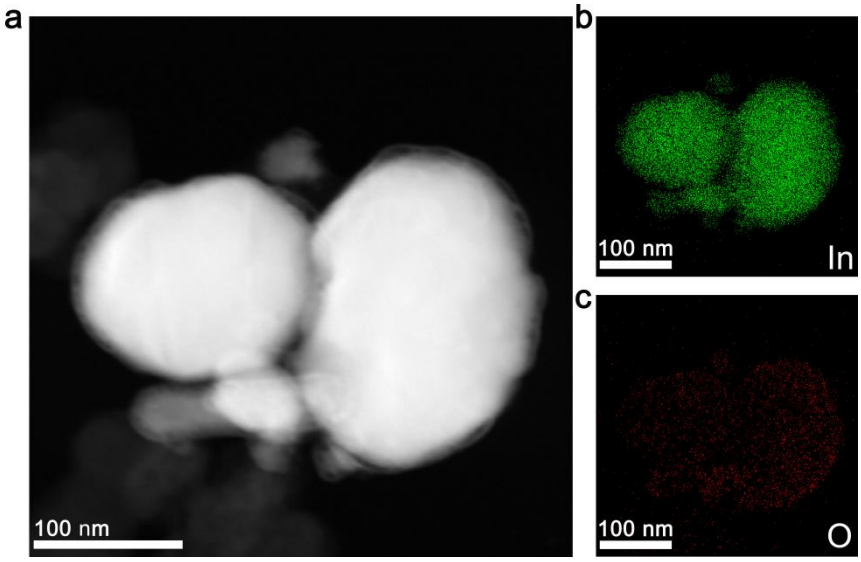
Supplementary Fig. 7 | XRD patterns of the pre-catalyst of s-LA-ITO, m-LA-IO and w-LA-ITO.



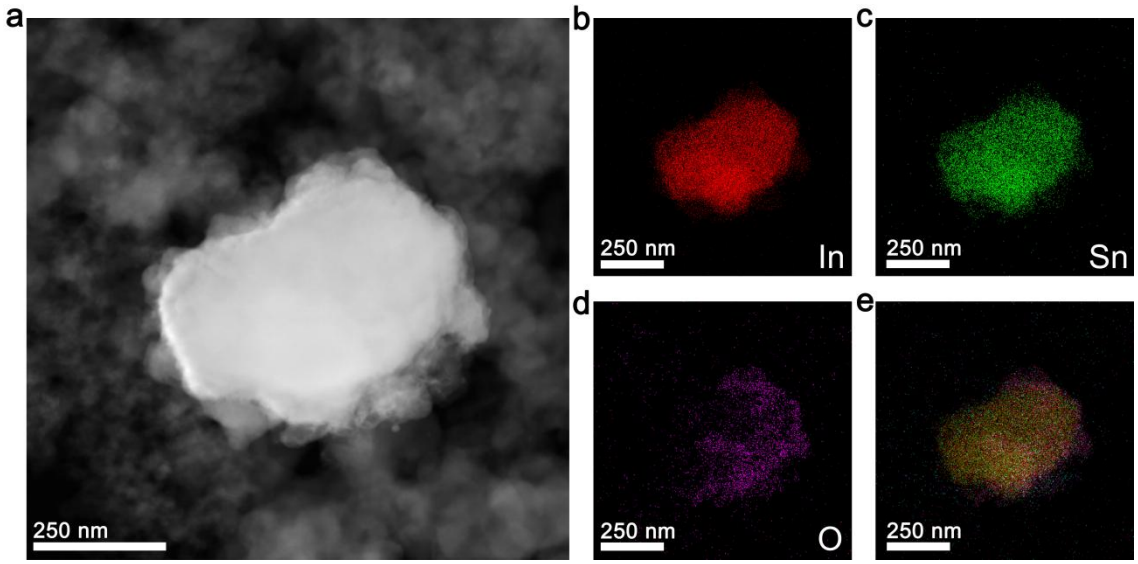
Supplementary Fig. 8 | XRD patterns of **a** AR-ITO, **b** AR-IO and **c** R-ITO.



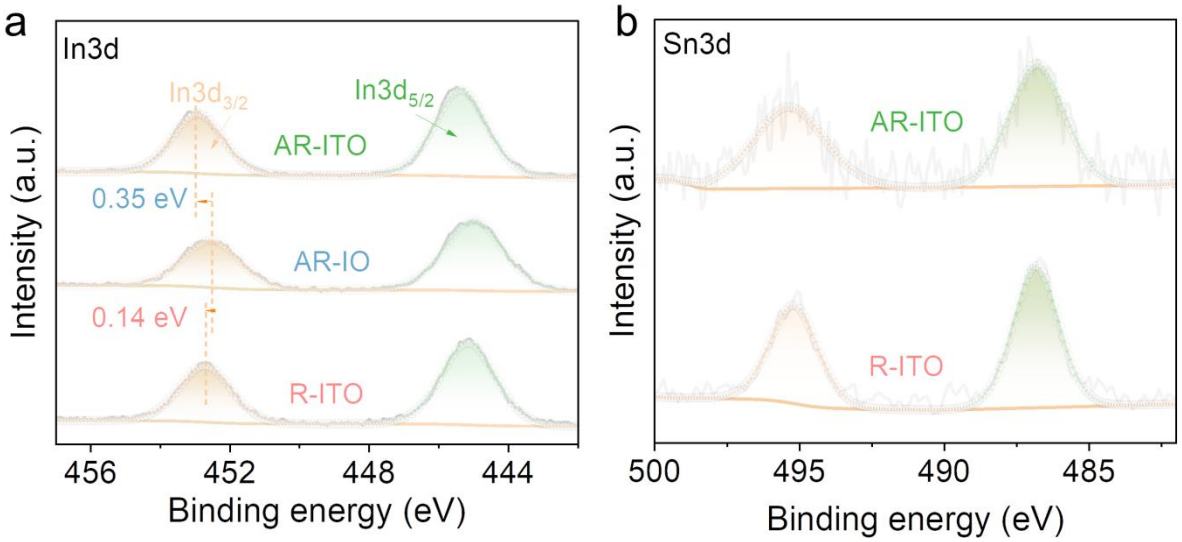
Supplementary Fig. 9 | XRD patterns of AR-ITO, AR-IO and R-ITO after the operating in a MEA for 50 h and 1500 h at 300 mA cm^{-2}.



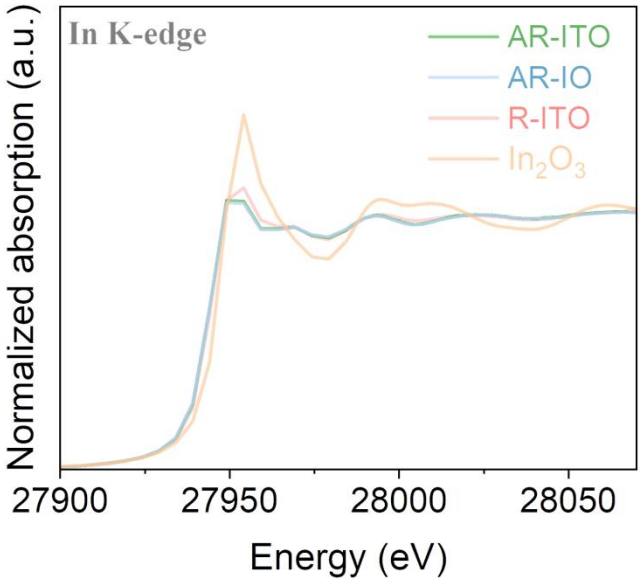
Supplementary Fig. 10 | **a** HR-TEM image and **b-c** EDS elemental mapping images of the AR-IO.



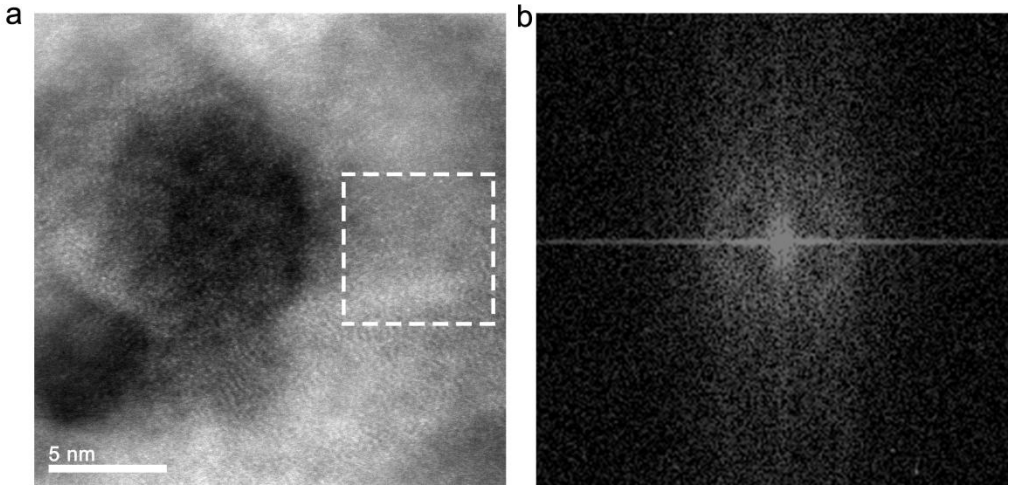
Supplementary Fig. 11 | **a** HR-TEM image and **b-e** EDS elemental mapping images of the R-ITO.



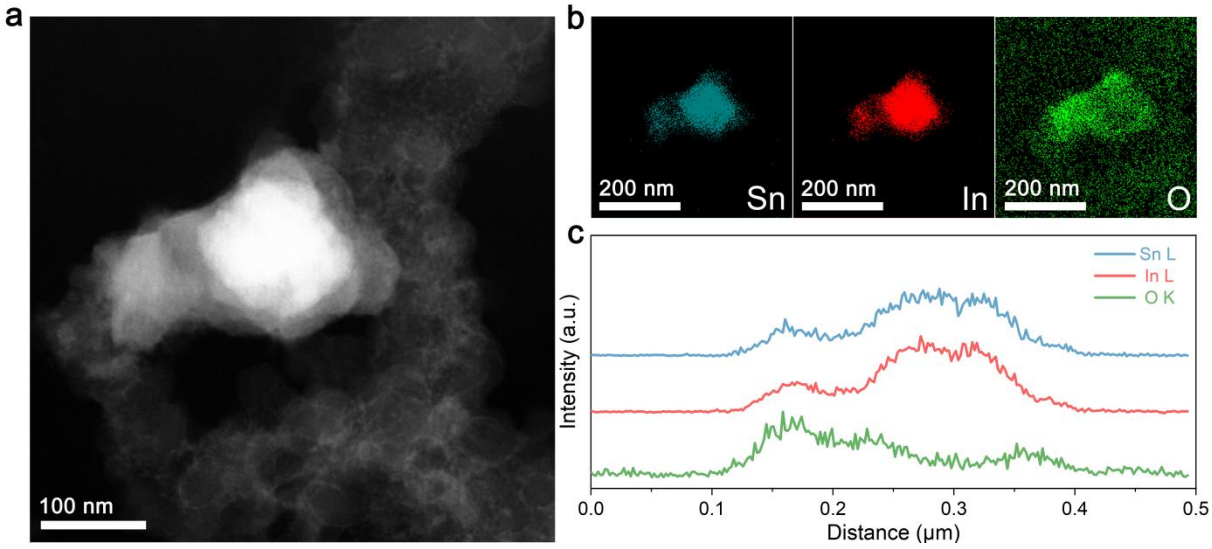
Supplementary Fig. 12 | **a** In 3d and **b** Sn 3d XPS spectra of AR-ITO, AR-IO and R-ITO.



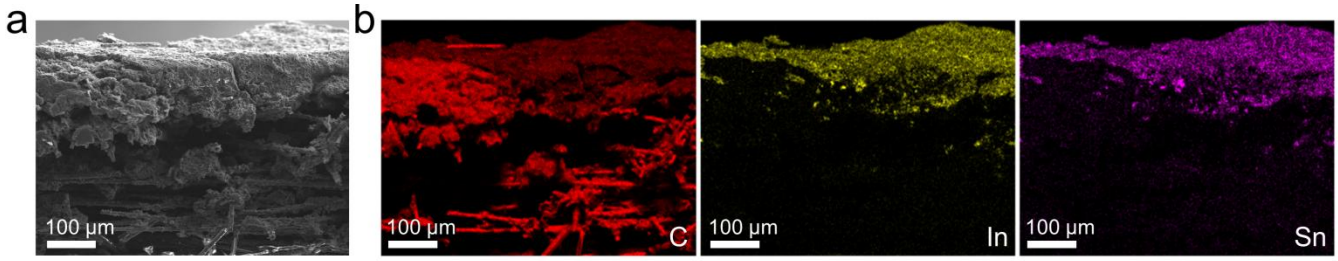
Supplementary Fig. 13 | Normalized In *k*-edge XANES spectra of AR-ITO, AR-IO, R-ITO and In_2O_3.



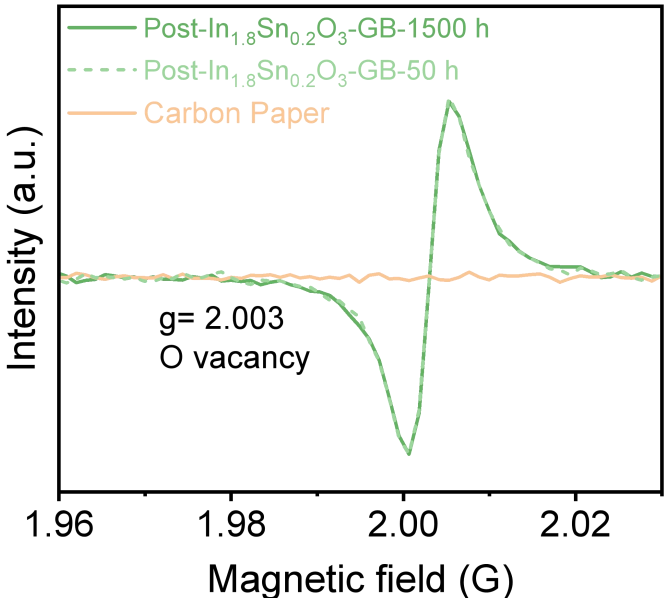
Supplementary Fig. 14 | **a** HAADF-STEM image of AR-ITO after operating in a MEA for 1500 h at 300 mA cm^{-2}. **b** The corresponding FFT image of the marked area in **a**.



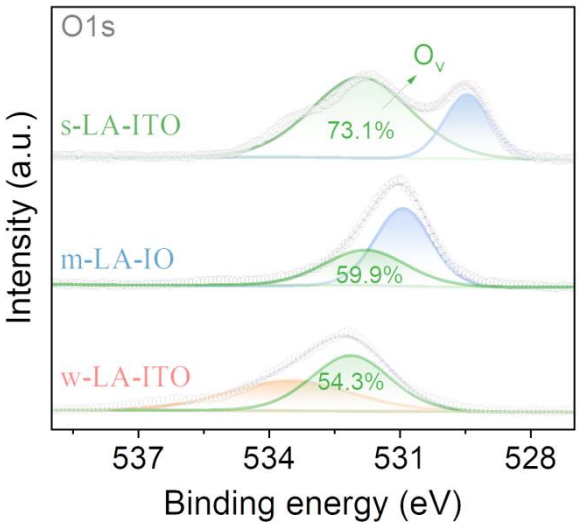
Supplementary Fig. 15 | **a** HR-TEM image, **b** EDS mapping images and **c** EDS line scan of AR-ITO after operating in a MEA for 1500 h at 300 mA cm^{-2}.



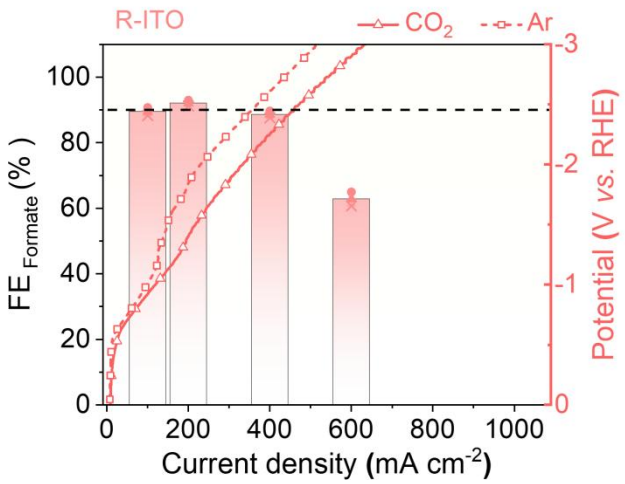
Supplementary Fig. 16 | **a** Cross-sectional SEM image of AR-ITO-GDE. **b** Corresponding EDS elemental mapping images of AR-ITO-GDE.



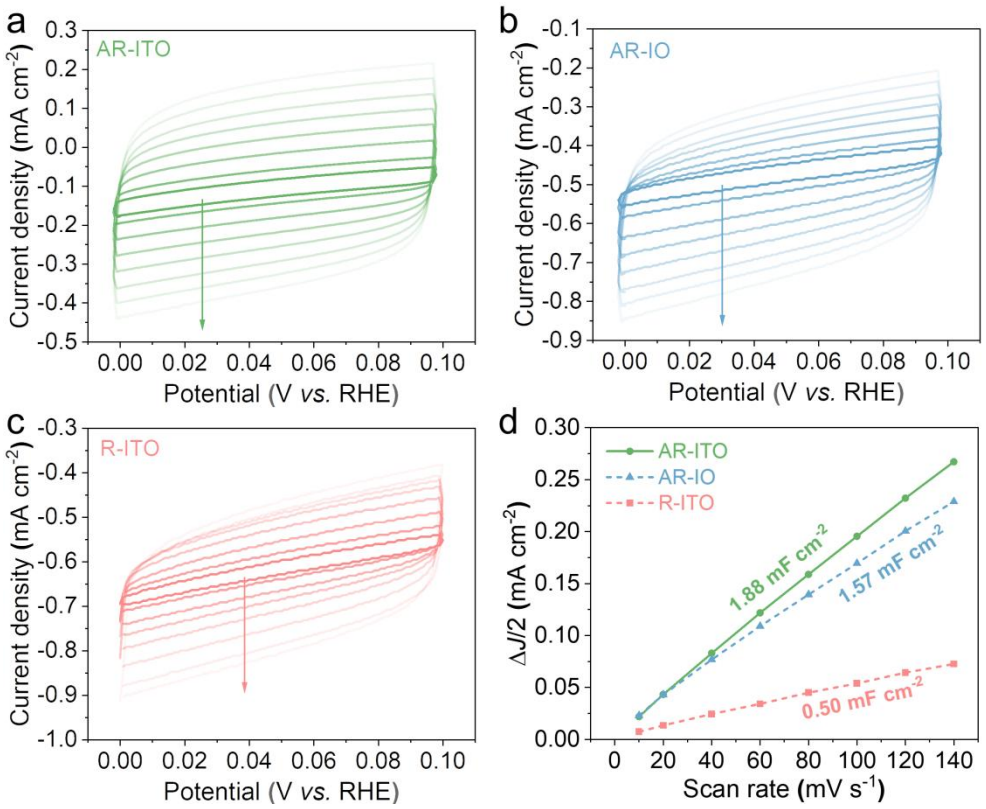
Supplementary Fig. 17 | EPR spectra of AR-ITO after operating in a MEA for 50 h and 1500 h at 300 mA cm^{-2}.



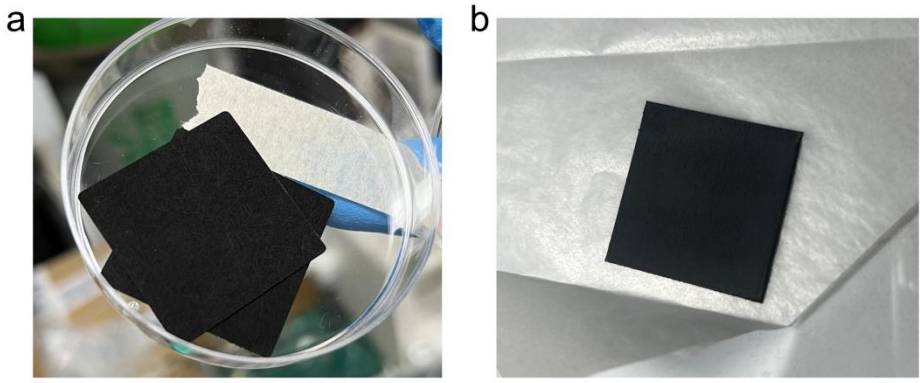
Supplementary Fig. 18 | O 1*s* XPS spectra of s-LA-ITO, m-LA-IO and w-LA-ITO.



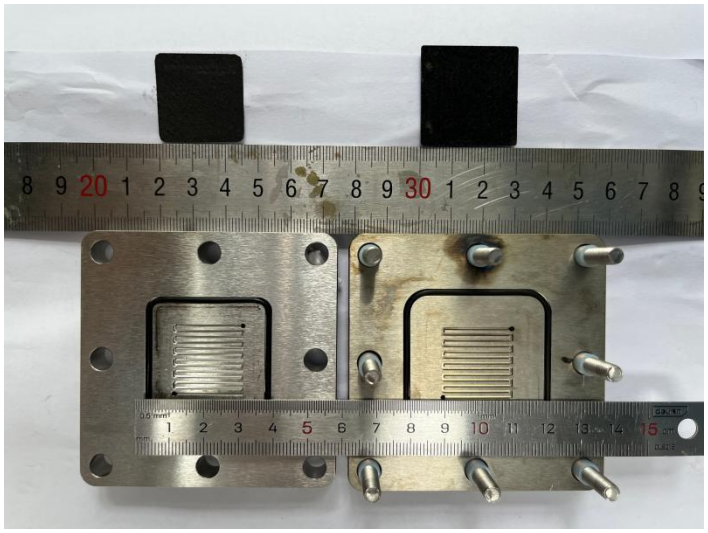
Supplementary Fig. 19 | Polarization curves over R-ITO under Ar (dashed line) and CO_2 (solid line) atmospheres in 0.5 M $KHCO_3$, and FE of formate on R-ITO with various current densities in 0.5 M $KHCO_3$ in a flow cell.



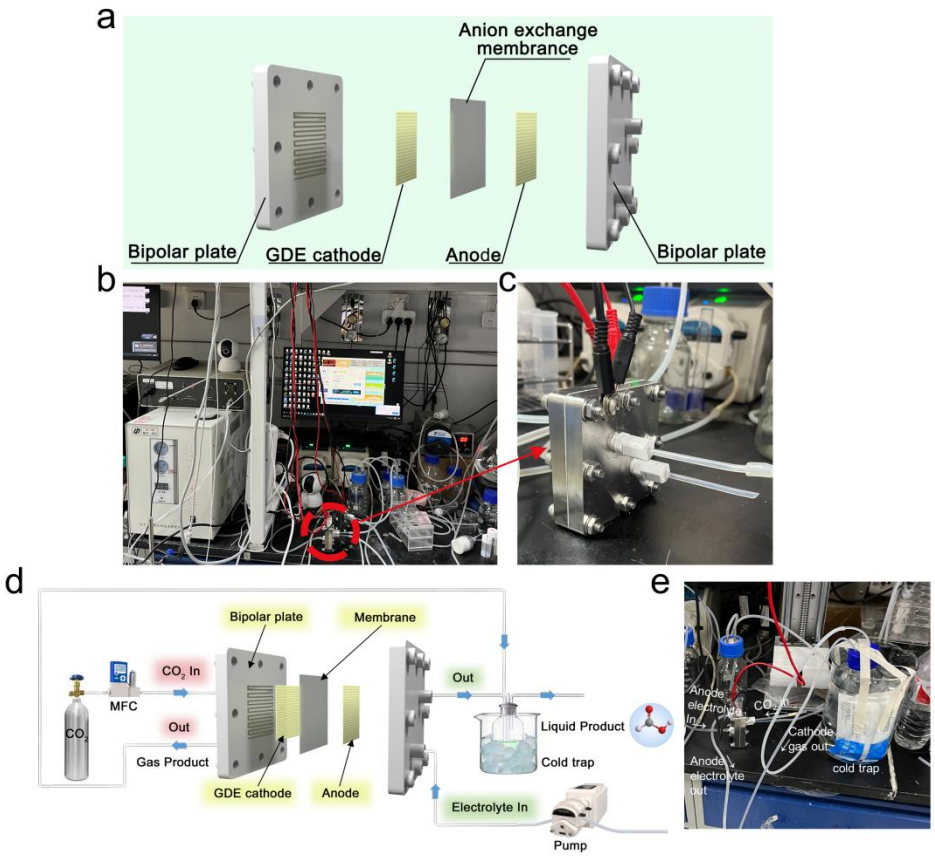
Supplementary Fig. 20 | **a-c** CVs of AR-ITO (**a**), AR-IO (**b**) and R-ITO (**c**) over a range of scan rates at 10-140 mV s^{-1}. **d** Current densities at various scan rates.



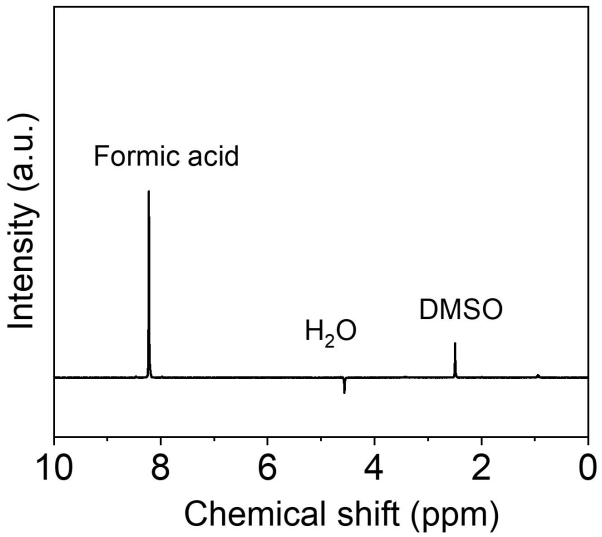
Supplementary Fig. 21 | Photos of the anode (**a**) and cathode (**b**) in MEA electrolyzers.



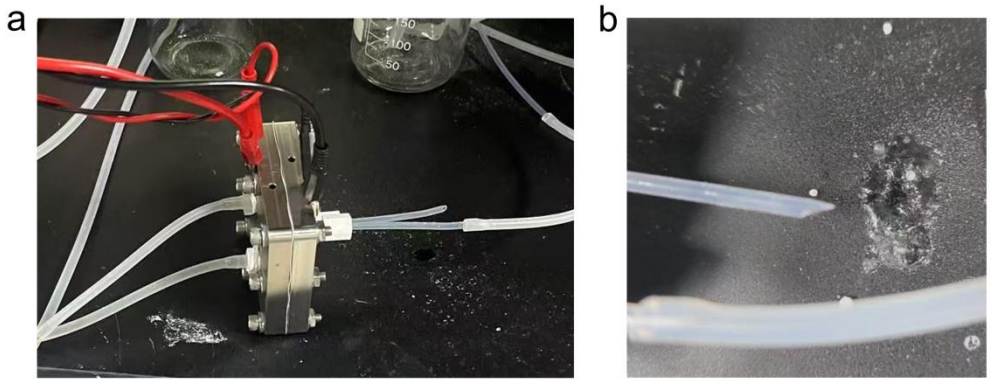
Supplementary Fig. 22 | Front view of cathode flow plate (bottom left) and anode flow plate (bottom right) with the same MEA cell active area of 5 cm^{-2} based on the area of the same size of electrode flow area. Photos of the 2.5 cm*2.5 cm cathode of carbon paper (top left) and 3 cm*3 cm anode of titanium felt (top right)) in MEA electrolyzers.



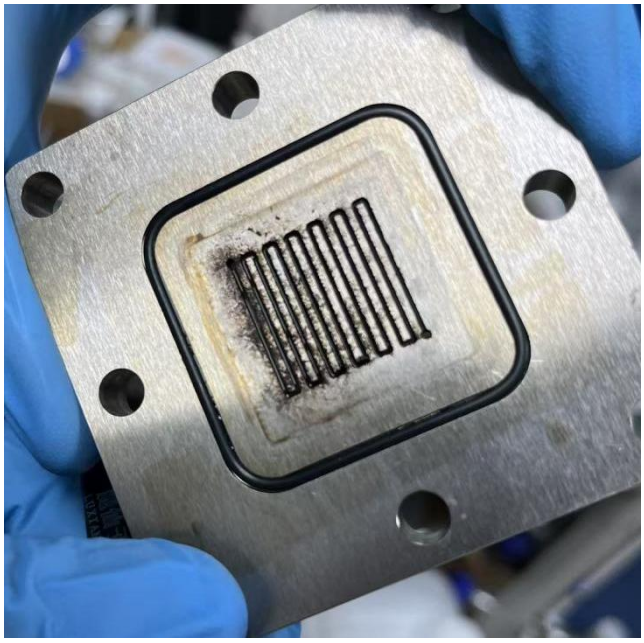
Supplementary Fig. 23 | **a** The schematic illustration of the MEA electrolyzer. **b-c** Photos of MEA electrolyzers. **d** Schematic illustration of the MEA setup. A cold trap was placed downstream of the effluent gas at the cathode to collect liquid products. **e** A photo of MEA electrolyzers with a cold trap.



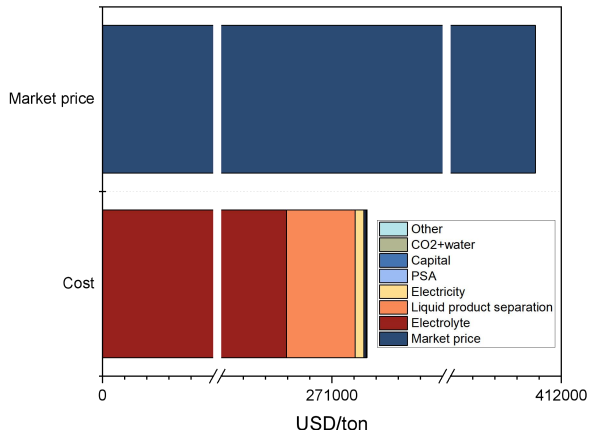
Supplementary Fig. 24 | ^{1}H-NMR spectrum of liquid products of AR-ITO.



Supplementary Fig. 25 | Salt precipitation observed at cathode outlet during the long-term operation (**a**), entrained by gas flow (**b**).



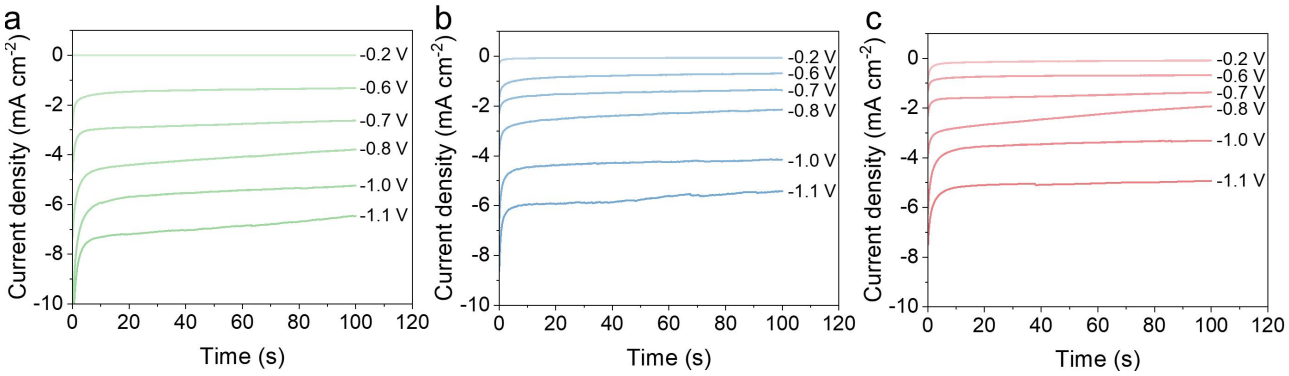
Supplementary Fig. 26 | The corroded anode plate by the electrolyte after operating in a MEA for 1500 h at 300 mA cm^{-2}.



Supplementary Fig. 27 | Market price and component analysis comparison of AR-ITO-based MEA electrolyzer.

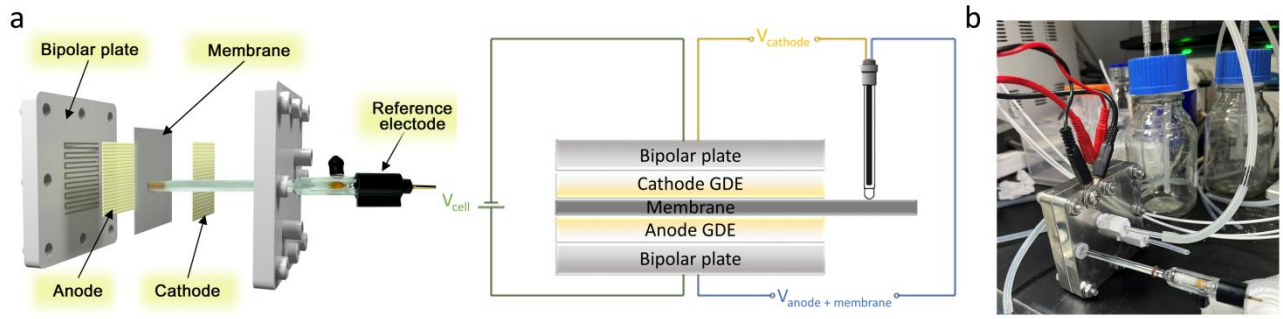


Supplementary Fig. 28 | A customized spectroelectrochemical cell with a three-electrode configuration was employed for all *in-situ* SEIRAS experiments.

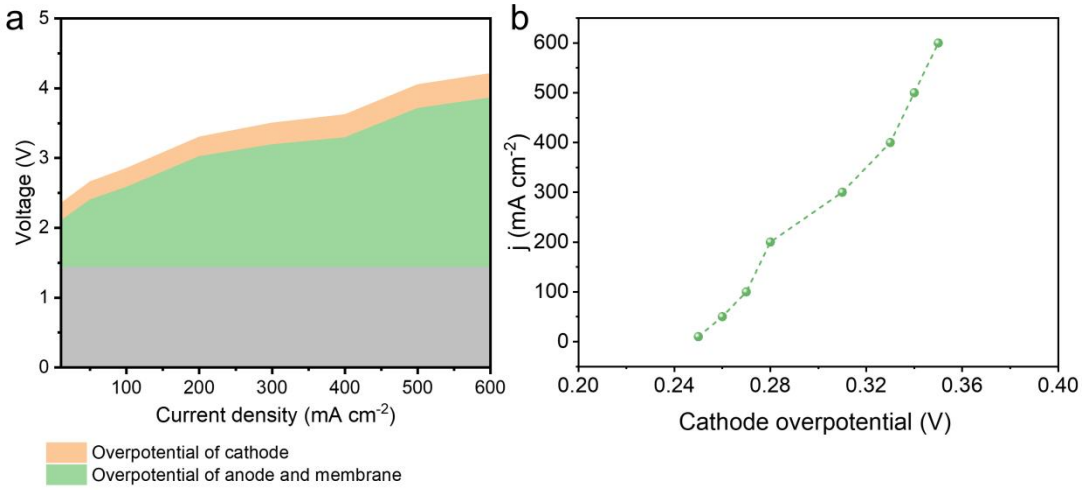


Supplementary Fig. 29 | The i-t curves of CO_2RR in H-type cell on s-LA-ITO (**a**), m-LA-IO (**b**) and w-LA-ITO (**c**).

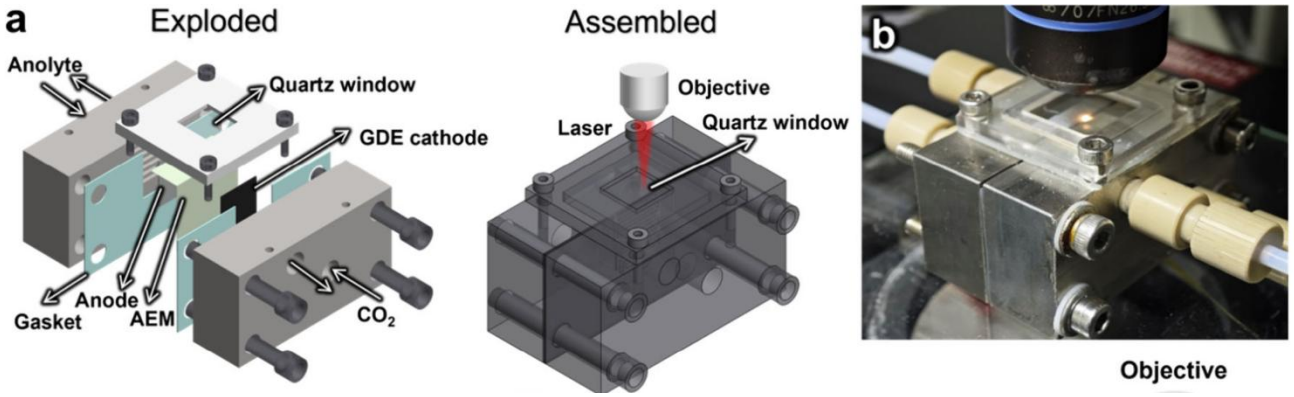
Here, an H-type cell configuration was employed for *in situ* ATR-SEIRAS measurements, and the current density (around 10 mA cm^{-2}) was thus inherently lower than that in flow-cell electrolyzers, as CO_2 supply was diffusion-limited.



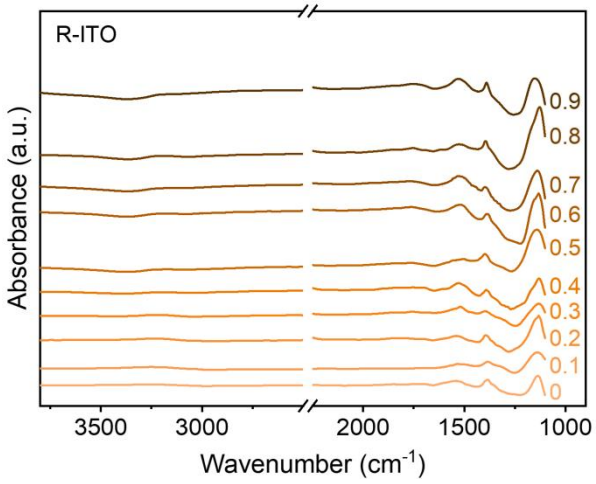
Supplementary Fig. 30 | **a** The voltammetric performance breakdown analysis for the MEA electrolyser (left). Schematic diagram showing the integration of the reference electrode in the MEA electrolyser (middle). **b** A photograph of the three-electrode MEA electrolyser.



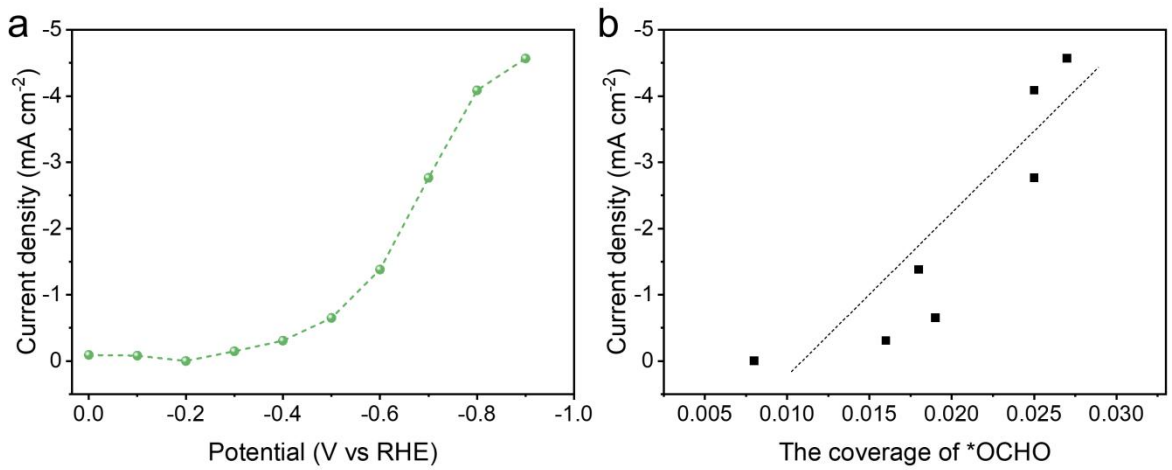
Supplementary Fig. 31 | **a** Voltage drops at different locations over the AR-ITO catalyst. **b** Current densities under different cathode over-potentials over the AR-ITO catalyst.



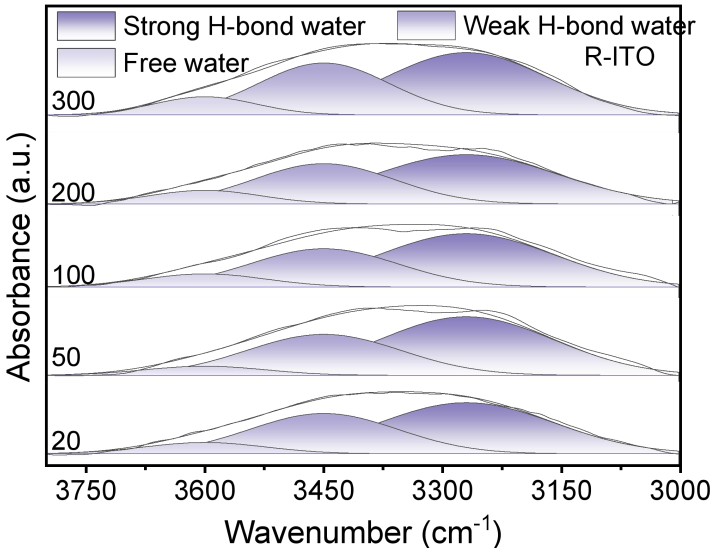
Supplementary Fig. 32 | **a** Schematic showing the exploded and assembled views of the *operando* Raman cell under MEA conditions. **b** Photograph of the assembled Raman cell during measurement. (*Operando* Raman spectra were acquired in a custom-designed spectroelectrochemical MEA cell following a previously reported configuration. *ACS Energy Lett*. 2025 10, 3445).



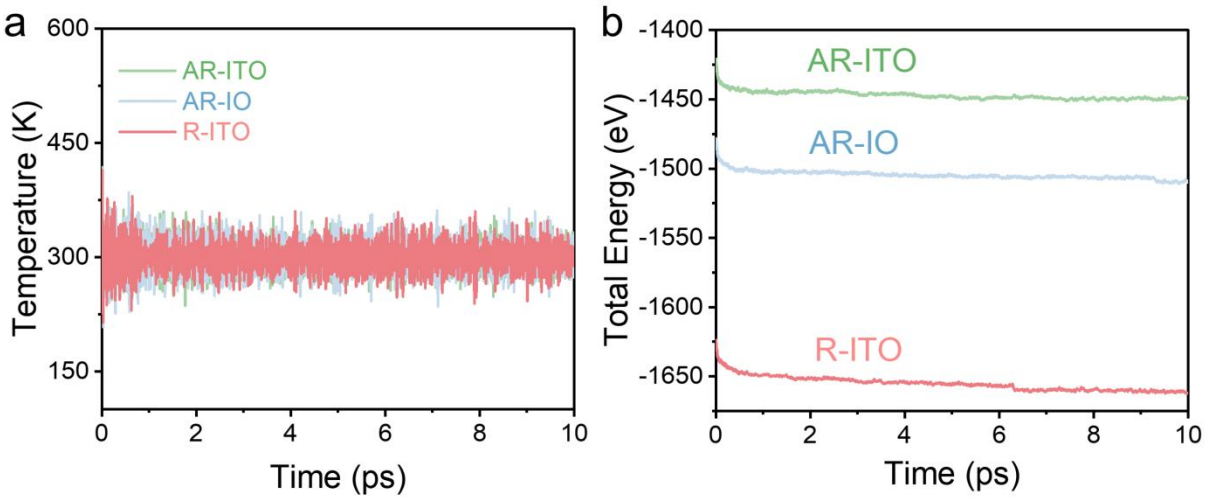
Supplementary Fig. 33 | Potential-dependent *in situ* ATR-SEIRAS spectra over the R-ITO catalyst.



Supplementary Fig. 34 | **a** The relationship between the current density and applied potential over the AR-ITO catalysts in *in-situ* ATR-SEIRAS measurements. **b** A linear-like relationship between current density and the coverage of *OCHO at around 1377 cm^{-1}.



Supplementary Fig. 35 | Fitted bands of interfacial water at various potentials from 3800 to 3000 cm^{-1} over the R-ITO catalysts.

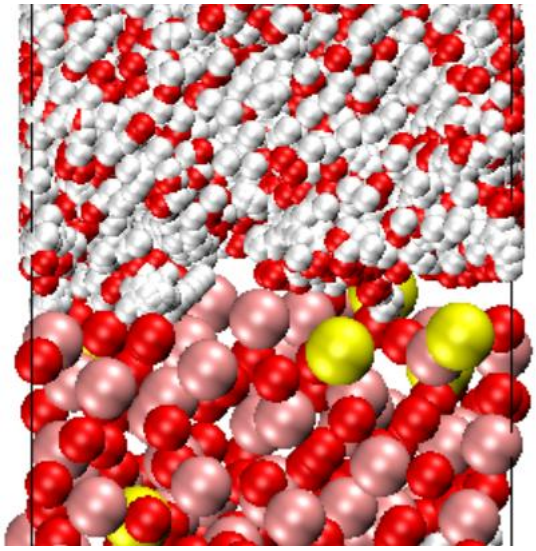


Supplementary Fig. 36 | **a** Temperature as a function of time. **b** Total energy as a function of time.

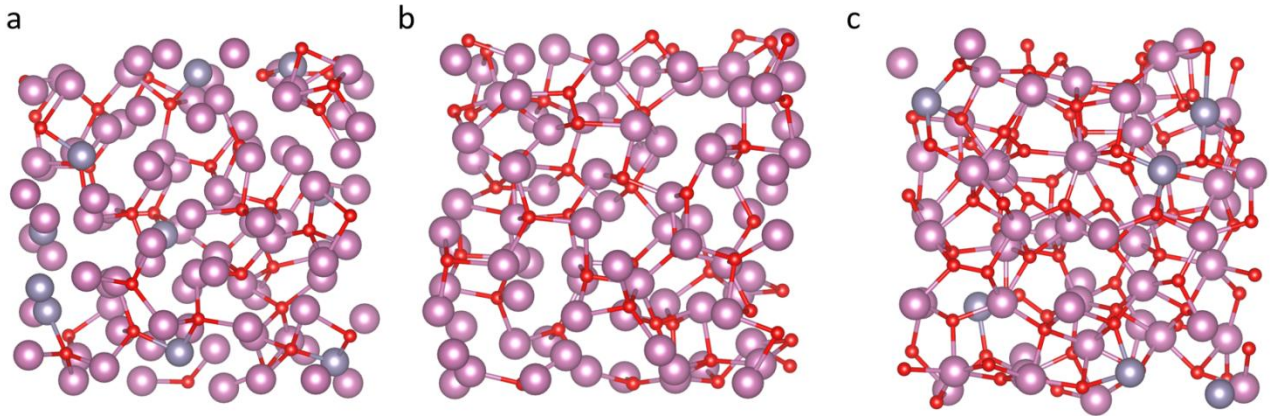
We analyzed our AIMD results for the three simulated systems.

First, the overall system temperature remained stable around the target value of 300 K throughout the simulation process, with typical fluctuations but no systematic drifts, as shown in the attached temperature-time plot (**Supplementary Fig. 36 a**). This indicates effective thermal control.

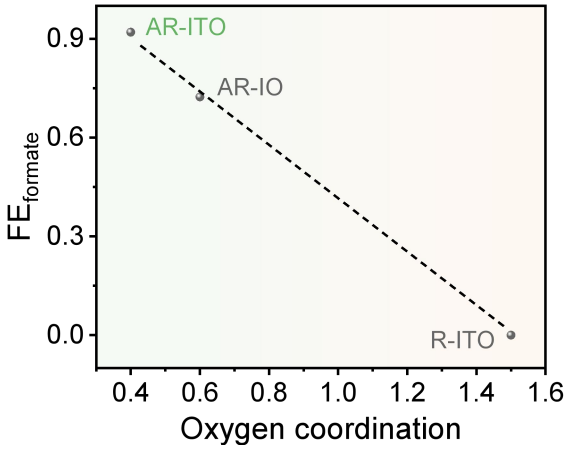
Additionally, the total energy profiles (**Supplementary Fig. 36 b**) show convergence to stable values without drifts, further confirming the reliability of the thermostatting in our simulations.



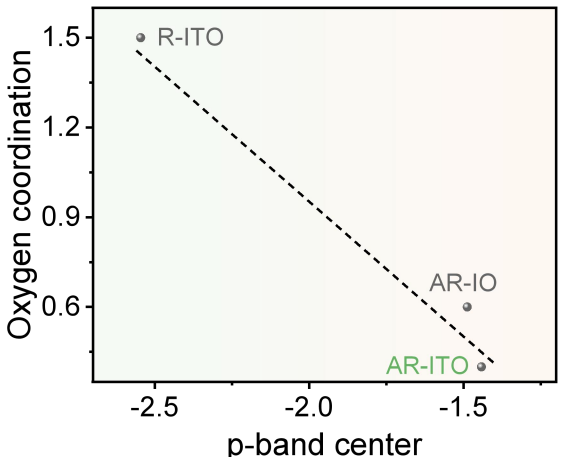
Supplementary Fig. 37 | Representative snapshot of the AIMD-simulated interface structure over the R-ITO catalysts.



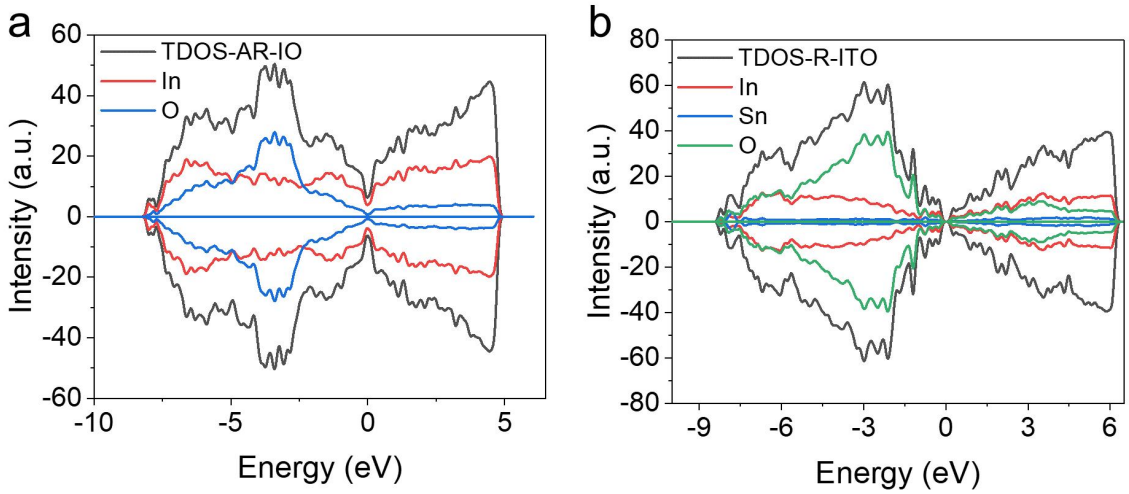
Supplementary Fig. 38 | **a-c** The configurations of AR-ITO (**a**), AR-IO (**b**) and R-ITO (**c**) models.



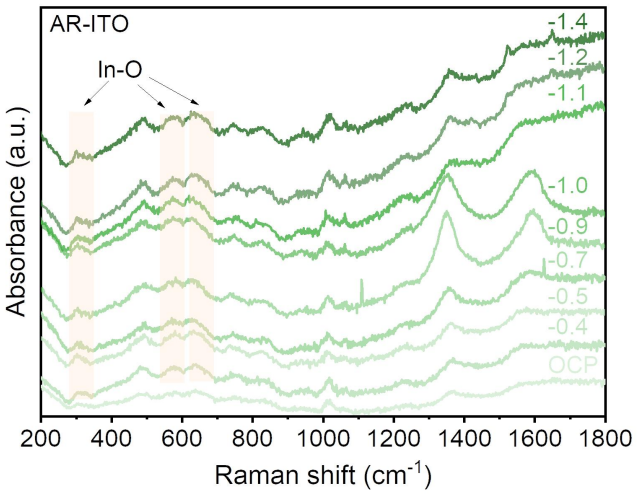
Supplementary Fig. 39 | A linear-like relationship between oxygen coordination and FE of formate at 800 mA cm^{-2}.



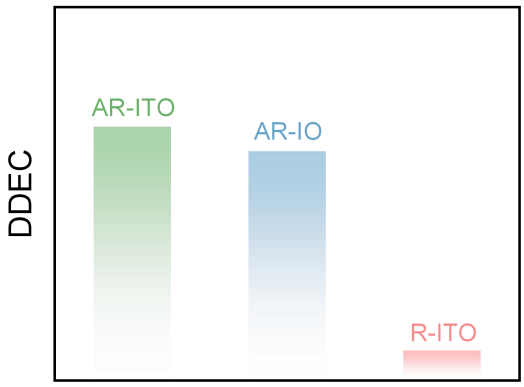
Supplementary Fig. 40 | p-band center-dependent oxygen coordination.



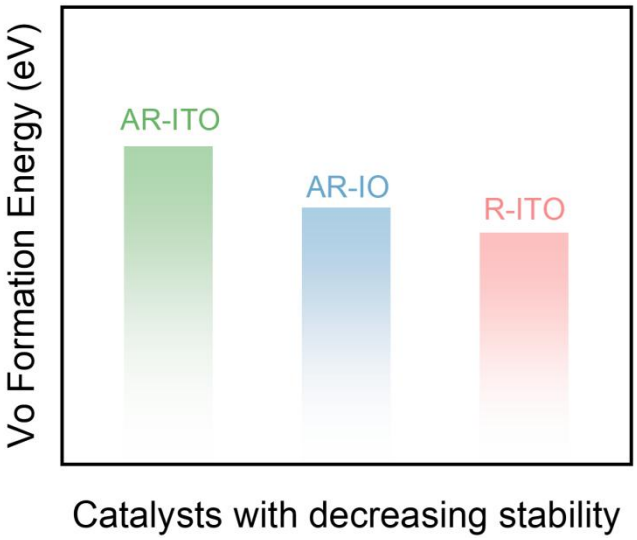
Supplementary Fig. 41 | TDOS for AR-IO (**a**), and R-ITO (**b**).



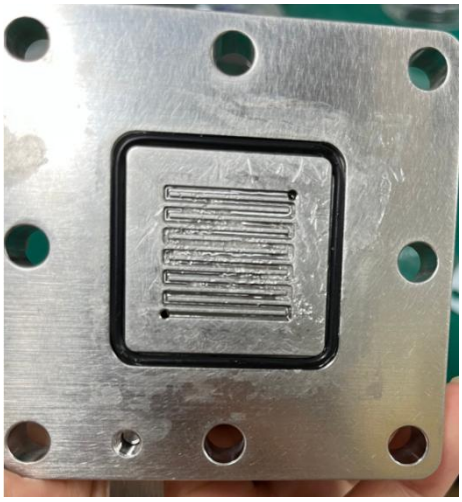
Supplementary Fig. 42 | Potential-dependent *in situ* Raman spectra over the AR-ITO.



Supplementary Fig. 43 | Oxygen DDEC bond order as a function of these catalysts.



Supplementary Fig. 44 | Vacancy formation energy for AR-ITO, AR-IO, and R-ITO.



Supplementary Fig. 45 | The cathode plate after operating in a MEA over R-ITO.

Tables

Supplementary Table 1 | Metal contents in s-LA-ITO and w-LA-ITO.

Sample	ICP (at%)	
	In	Sn
s-LA-ITO	0.92	0.08
w-LA-ITO	0.91	0.09

Supplementary Table 2 | Curve fitting parameters for In *k*-edge EXAFS of AR-ITO, AR-IO, R-ITO and In_2O_3.

Materials	Path	*N*	*R*/Å	$\sigma^2/(10^{-3}Å^2)$	E_0/eV	*R* factor
In_2O_3	In-O	6	2.16			
	In-O-In	6	3.36			
	In-O-In	6	3.82			
R-ITO	In-O	1.5 ± 0.1	2.14 ± 0.01	0.005 ± 0.002	6 ± 1	0.004
	In-In (metallic In)	4.5 ± 0.8	3.21±0.05	0.021 ± 0.003	1 ± 1	
	In-O-In	2.7 ± 1.1	3.87 ± 0.05	0.021 ± 0.003		
AR-IO	In-O	0.6 ± 0.1	2.11 ± 0.02	0.002 ± 0.002	3 ± 3	0.027
	In-In (metallic In)	6.7 ± 2.4	3.20 ± 0.04	0.028 ± 0.006	2 ± 1	
	In-O-In	5.0 ± 3.6	3.82 ± 0.07	0.028 ± 0.006		
AR-ITO	In-O	0.4 ± 0.2	2.09 ± 0.05	0.001 ± 0.001	-1 ± 7	0.040
	In-In (metallic In)	4.7 ± 1.7	3.25 ± 0.04	0.020 ± 0.005	3 ± 2	
	In-O-In	2.9 ± 2.1	3.89 ± 0.09	0.020 ± 0.005		

[a]S_0^2 was fixed as 0.99. Data ranges: $3 \leq k \leq 10$ Å, $1.0 < R < 4.0$ Å. The number of variable parameters is 10, out of a total of 14 independent data points. N, coordination number; R, bond length; σ^2 Debye-Waller factor; ΔE_0 inner potential shift.

Supplementary Table 3 | Assignments of *in situ* ATR-SEIRAS bands observed in **Figure 5**.

Wavenumbers/cm^{-1}	assignments
~1130	π(C-H) of formate
~1220	ν(C-O) of formate
~1250	$*CO_2^{\cdot-}$
~1377	ν(O-C-O) of symmetric *OCHO
~1540	ν(O-C-O) of asymmetric *OCHO
~1645	δ(H-O-H) of interfacial water
~1690	$*CO_2^{\cdot-}$
~1740	ν(C=O) of formate
3000~3700	ν(O-H) of H_2O

ν: stretching vibration; δ: bending vibration; π: out-of-plane bending vibration.

Supplementary Table 4 | DDEC bond order for AR-ITO, AR-IO, and R-ITO.

Model	O
AR-ITO	2.066
AR-IO	2.061
R-ITO	2.021

References

1. Zhang, Y. et al. Low-coordinated copper facilitates the *CH_2CO affinity at enhanced rectifying interface of Cu/Cu_2O for efficient CO_2-to-multicarbon alcohols conversion. *Nat. Commun.* **15**, 5172 (2024).
2. Ma, Z. et al. CO_2 electroreduction to multicarbon products in strongly acidic electrolyte *via* synergistically modulating the local microenvironment. *Nat. Commun.* **13**, 7596 (2022).
3. Ye, F. et al. The role of oxygen-vacancy in bifunctional indium oxyhydroxide catalysts for electrochemical coupling of biomass valorization with CO_2 conversion. *Nat. Commun.* **14**, 2040 (2023).
4. Chen, Y. et al. Efficient multicarbon formation in acidic CO_2 reduction *via* tandem electrocatalysis. *Nat. Nanotechnol.* **19**, 311-318 (2024).
5. Liu, T. et al. A Tin Oxide-Coated Copper Foam Hybridized with a Gas Diffusion Electrode for Efficient CO_2 Reduction to Formate with a Current Density Exceeding 1 A cm^{-2}. *Small*. **18**, 2205323 (2022).
6. Kresse, G. et al. Efficiency of ab-initio total energy calculations for metals and semiconductors using a plane-wave basis set. *Comput. Mater. Sci.* **6**, 15-50 (1996).
7. Burke, K. et al. Generalized Gradient Approximation Made Simple. *Phys. Rev. Lett.* **77**, 3865-3868 (1996).
8. Nørskov, J. K. et al. Origin of the Overpotential for Oxygen Reduction at a Fuel-Cell Cathode. *J. Phys. Chem. B*. **108**, 17886-17892 (2004).
9. Mathew, K. et al. Implicit solvation model for density-functional study of nanocrystal surfaces and reaction pathways. *J. Chem. Phys*. **140**, 84106 (2014).
10. Kresse, G. & Joubert, D. P. From ultrasoft pseudopotentials to the projector augmented-wave method. *Phys. Rev. B*. **59**, 1758-1775 (1999).
11. Hua, Y. et al. Electrified CO_2 -to-HCOOH Valorization: A Comparative Technical Analysis on Acidic Flow Cell and Solid-State Electrolyte Cell Reactors. *Acs Energy Lett.* **11**, 1880-1888 (2026).
12. Huang, L., Gao, G., Zhao, J., Roberts, W. L. & Lu, X. Electrocatalytic upcycling of high-pressure captured CO_2 to ethylene. *Nat. Catal.* **8**, 968-976 (2025).
13. Li, J. et al. A high-flux membrane electrode assembly for CO_2 electroreduction to 4.5 M formate with over 8,000 h stability. *Nat. Catal.* **9**, 492-501 (2026).
14. Liu, J., Chen, D., Tang, T. & Sun, L. Green chemical process for continuous production of high-purity 2,5-furandicarboxylic acid in anion exchange membrane flow electrolyzer. *Nat. Commun.* **17**, 2099 (2026).
15. Fang, W. et al. Durable CO_2 conversion in the proton-exchange membrane system. *Nature*. **626**, 86-91 (2024).
16. She, X. et al. Kilowatt-scale alkali-cation-free CO_2 electrolysis via accelerating mass transfer. *Nat. Commun.* **17**, 2641 (2026).
17. Shin, H., Hansen, K. U. & Jiao, F. Techno-economic assessment of low-temperature carbon dioxide electrolysis. *Nat. Sustain.* **4**, 911-919 (2021).
18. Wu, T. et al. Electrolysis with built-in seawater desalination by porous-solid-electrolyte reactor. *Nat. Sustain.* **9**, 523-532 (2026).
19. Wang, X. et al. Efficient electrosynthesis of n-propanol from carbon monoxide using a Ag-Ru-Cu catalyst. *Nat. Energy*. **7**, 170-176 (2022).

20. Chen, X. et al. Comparative techno-economic analysis of saline wastewater resourceful utilization: Impurity removal-salt extraction vs. impurity removal-electrolysis. *Chem. Eng. J.* **519**, 165511 (2025).
21. Liu, H., Sun, X., Gao, F., Zheng, Y. & Qiao, S. Cost-efficient and stable electrolysis of reverse osmosis water using a Co-RuO_2-enabled PEM electrolyser. *Nat. Catal.* **9**, 9-17 (2026).